

Double Higgcison:**125 GeV Higgs boson and a potential diphoton Resonance**Kingman Cheung^{1,2,3}, P. Ko⁴, Jae Sik Lee^{5,3}, Jubin Park^{4,5,3}, and Po-Yan Tseng^{6,1}¹ *Department of Physics, National Tsing Hua University, Hsinchu 300, Taiwan*² *Division of Quantum Phases and Devices, School of Physics,
Konkuk University, Seoul 143-701, Republic of Korea*³ *Physics Division, National Center for Theoretical Sciences, Hsinchu, Taiwan*⁴ *School of Physics, KIAS, Seoul 130-722, Republic of Korea*⁵ *Department of Physics, Chonnam National University,
300 Yongbong-dong, Buk-gu, Gwangju, 500-757, Republic of Korea*⁶ *Kavli IPMU (WPI), UTIAS, University of Tokyo, Kashiwa, 277-8583, Japan*

(Dated: August 16, 2016)

Abstract

Searches for diphoton resonance have been shown to be very useful in discovering new heavy spin-0 or spin-2 particles. Supposing that a new heavy particle shows up in the diphoton channel and it points to a spin-0 boson, it can be allowed to have a small mixing with the observed 125 GeV Higgs-like boson. We borrow the example of the 750 GeV particles hinted with 3.2 fb^{-1} data at the end of 2015 (though it did not appear in the 2016 data) to perform an analysis of “double Higgcison”. In this work, we perform a complete Higgs-signal strength analysis in the Higgs-portal type framework, using all the existing 125 GeV Higgs boson data as well as the diphoton signal strength of the 750 GeV scalar boson. The best fit prefers a very tiny mixing between two scalar bosons, which has to be accommodated in models for the 750 GeV scalar boson.

I. INTRODUCTION

The first run at $\sqrt{s} = 13$ TeV at the LHC has hinted a possibility of observing a new particle at around 750 GeV. Both ATLAS and CMS collaborations have reported a “bump” in the diphoton invariant mass distribution around 750 GeV, indicating a local significance of 3.9σ by ATLAS [1] and about 3σ by the CMS [2]. Such an excitement has motivated a lot of speculations in many theories. Everyone has very high expectation for the new run coming up in May 2016 at the LHC.

Both ATLAS and CMS updated their findings in the early 2016 during the Moriond Conference. In particular, the CMS also included a set of data without the magnetic field into the analysis, and improved the significance to about 3.2σ . The summary of the diphoton data of the 750 GeV resonance is given in Table I. Although the hint is preliminary, it has stimulated a lot of phenomenological activities, bringing in a number of models for interpretation. * If the particle decays directly into a pair of photons, it can have a spin-0 or spin-2, however, one has to entertain the possibility that the 750 GeV particle undergoes cascade decays into collimated photon objects (aka photon-jets) [3].

During the ICHEP 2016 conference, both ATLAS and CMS reported their searches including the new 2016 data totaling about $12\text{--}13\text{ fb}^{-1}$ [4]. The ATLAS collaboration reanalyzed the 2015 data of 3.2 fb^{-1} and they reported a little bit smaller excess of 3.4σ at 730 GeV, compared to the previous 3.9σ excess at 750 GeV. While, in the new 2016 data of 12.2 fb^{-1} , they have not observed any significant excess at all. In the combined data of 15.4 fb^{-1} , they observed 2.3σ excess at 710 GeV for the wide width case with $\Gamma_X/m_X=10\%$. In the narrow width case, the combined data show several $\sim 2\sigma$ excesses with the largest one at 1.6 TeV with a 2.4σ local significance. The CMS collaboration has observed no significant excess in proximity of 750 GeV in the new 2016 data of 12.9 fb^{-1} , either. But, interestingly, it reported the largest excess newly appeared at 620 GeV with $\sim 2.4\text{--}2.7\sigma$ local significance. And, like as in the ATLAS case, the combined $\sqrt{s} = 13$ TeV data of $16.2/\text{fb}$ show several excesses at the level of $\sim 2\sigma$.

Both experiments did not further find evidence of the 750 GeV resonance. Nevertheless, we do not give up. Hints of new particles can easily show up in the near future data. For example, the CMS data in ICHEP 2016 showed a new 2σ effect at around 620–650 GeV.

* There has been more than 300 articles appearing on arXiv that interpret the 750 GeV particle. We only refer to those relevant to our work here.

The ATLAS, on the other hand, did not see any new diphoton resonance in the new 13 TeV data but still there was 3.4σ effect around 730 GeV in the 2015 data. Under this situation, there are often possibilities that potentially heavy diphoton resonances can show up in the near future. We borrow the example of the 750 GeV particles hinted with 3.2 fb^{-1} data at the end of 2015 (though it did not appear in the 2016 data) to perform an analysis of “double Higgscision” – the precision-coupling analysis involving both Higgs bosons.

In this work, we focus on the interpretation that this 750 GeV particle is a scalar boson that links the SM sector with the hidden sector through the Higgs-portal type interactions, in which an $SU(2)$ isospin-singlet scalar boson mixes with the SM Higgs boson through an angle α [5]. We assume after mixing the lighter boson is the observed SM-like Higgs boson H_1 at 125 GeV while the heavier one H_2 is the one hinted at 750 GeV. Thus, the 750 GeV scalar boson H_2 opens the window to another hidden world containing perhaps dark matter and other exotic particles.

In our previous global fits to the Higgs-portal type models with all the Higgs boson data from Run I [6] before the hint of the 750 GeV boson, we have constrained the parameter space of a few Higgs-portal singlet-scalar models. In those models without non-SM contributions to the $h\gamma\gamma$ and hgg vertices, the mixing angle is constrained to $\cos\alpha > 0.86$ at 95% CL. However, in those models with vector-like leptons (quarks) the mixing angle can be relaxed to $\cos\alpha > 0.83$ (0.7) at 95% CL. The implication was that the 750 GeV scalar boson H_2 can be produced in gg fusion as if it were a 750 GeV SM Higgs boson but with a suppression factor $\sin^2\alpha$ if there are no vector-like quarks running in the H_2gg vertex. Additional contributions arise when there are vector-like quarks running in the loop. Similarly, the decays of the scalar boson H_2 can be enhanced substantially into a pair of photons and gluons in the presence of vector-like fermions.

In an earlier attempt when the 750 GeV particle was first hinted, we performed such an analysis in the Higgs-portal framework that the 750 GeV boson H_2 interacts with the SM particles via the mixing angle with the 125 GeV Higgs boson and also via vector-like fermions [7]. Because the vector-like quarks carry electric and color charges while the vector-like leptons carry electric charges, the 750 GeV boson can be produced via gluon fusion and can also decay into a pair of photons and gluons. In [7] we used all the 125 GeV Higgs boson signal strength data and also the diphoton cross section of the 750 GeV boson to constrain the couplings of the 125 GeV Higgs boson, the mixing angle, and also on the extra loop

contributions to the 750 GeV boson due to the vector-like fermions.

In this work, we extend the earlier analysis into a full-swing analysis, taking into account various combinations of 125 GeV Higgs couplings, the 750 GeV boson couplings to vector-like fermions, and the mixing angle. Improvements are summarized as follows.

1. We include the effects of vector-like fermions in gluon fusion production and
2. We include the non-standard decay modes for the 750 GeV boson.
3. We separately consider the choices of narrow and wide width for the 750 GeV boson.

While the ATLAS data prefers a wide width, the CMS data prefers the narrow width.

The organization is as follows. In the next section, we describe briefly the framework of Higgs-portal models with vector-like fermions, including the production and decays of the 125 GeV and 750 GeV bosons. In Sec. III, we describe the Higgs boson and 750 GeV boson data that we use in our analysis, and We present the fits for various combinations of couplings and the mixing angle in Sec. IV. In Sec. V, we discuss the decay rates for the 750 GeV boson into other diboson channels (WW , ZZ and $Z\gamma$) when the vector-like quarks in the loop are weak doublets and/or weak singlets with arbitrary $U(1)_Y$ hypercharges. Then we conclude in Sec. VI.

Special note: After we posted this preprint to arXiv, both ATLAS and CMS announced that they did not find evidence of the 750 GeV resonance in the new 2016 data. We, nevertheless, think this double-Higgcision study would still be a good exercise whenever another diphoton resonance shows up in the future data. In the following, we shall borrow the data of the 750 GeV particles recorded with 3.2 fb^{-1} luminosity at the end of 2015 to perform an analysis of “double Higgcision” – the precision-coupling analysis involving both Higgs bosons.

II. FORMALISM

Interpreting the 750 GeV diphoton resonance as a scalar resonance generically involves at least two interaction eigenstates of h and s : h denotes the remnant of the SM Higgs doublet H and s the singlet or the remnant of additional Higgs doublets, triplets, etc. Then the two states h and s mix and result in the two mass eigenstates $H_{1,2}$. In the singlet case, for

example, the mixing is generated from renormalizable potential terms such as

$$V \supset \mu s H^\dagger H + \frac{\lambda}{2} s^2 H^\dagger H.$$

In this work, for concreteness, we concentrate on the singlet case.

A. Mixing and couplings

The mass eigenstates are related to the states h and s through an $SO(2)$ rotation as follows:

$$H_1 = h \cos \alpha - s \sin \alpha; \quad H_2 = h \sin \alpha + s \cos \alpha \quad (1)$$

with $\cos \alpha$ and $\sin \alpha$ describing the mixing between the interaction eigenstates h and s . In the limit of $\sin \alpha \rightarrow 0$, H_1 (H_2) becomes the pure doublet (singlet) state. In this work, we are taking H_1 for the 125 GeV boson discovered at the 8-TeV LHC run and H_2 for the 750 GeV state hinted at the early 13-TeV LHC run. We are taking $\cos \alpha > 0$ without loss of generality. For the detailed description of this class of models and also Higgs-portal models, we refer to Refs. [5, 6].

In this class of models, the singlet field s does not directly couple to the SM particles, but only through the mixing with the SM Higgs field at renormalizable level. The Yukawa interactions of h and s are described by

$$-\mathcal{L}_Y = h \sum_{f=t,b,\tau} \frac{m_f}{v} \bar{f} f + s \sum_{F=Q,L} g_{s\bar{F}F}^S \bar{F} F, \quad (2)$$

with f denoting the 3rd-generation SM fermions and F the extra vector-like fermions (VLFs): vector-like quarks (VLQs) and vector-like leptons (VLLs). Thus, the couplings of the two mass eigenstates $H_{1,2}$ to the SM fermions and VLFs are given by

$$\begin{aligned} -\mathcal{L}_Y = & H_1 \left[\cos \alpha \sum_{f=t,b,\tau} \frac{m_f}{v} \bar{f} f - \sin \alpha \sum_{F=Q,L} g_{s\bar{F}F}^S \bar{F} F \right] \\ & + H_2 \left[\sin \alpha \sum_{f=t,b,\tau} \frac{m_f}{v} \bar{f} f + \cos \alpha \sum_{F=Q,L} g_{s\bar{F}F}^S \bar{F} F \right]. \end{aligned} \quad (3)$$

Incidentally, the couplings to massive vector bosons $V = W, Z$ are given by

$$\mathcal{L}_{HVV} = g M_W \left(W_\mu^+ W^{-\mu} + \frac{1}{2c_W^2} Z_\mu Z^\mu \right) (\cos \alpha H_1 + \sin \alpha H_2). \quad (4)$$

The couplings of $H_{1,2}$ to two gluons, following the conventions and normalizations of Ref. [8], are given by

$$\begin{aligned}
S_{H_1}^g &= \cos \alpha S_{H_1}^{g(\text{SM})} - \sin \alpha S_{H_1}^{g(Q)} \\
&\equiv \cos \alpha \sum_{f=t,b} F_{sf}(\tau_{1f}) - \sin \alpha \sum_Q g_{s\bar{Q}Q}^S \frac{v}{m_Q} F_{sf}(\tau_{1Q}), \\
S_{H_2}^g &= \sin \alpha S_{H_2}^{g(\text{SM})} + \cos \alpha S_{H_2}^{g(Q)} \\
&\equiv \sin \alpha \sum_{f=t,b} F_{sf}(\tau_{2f}) + \cos \alpha \sum_Q g_{s\bar{Q}Q}^S \frac{v}{m_Q} F_{sf}(\tau_{2Q}), \tag{5}
\end{aligned}$$

where $\tau_{ix} = M_{H_i}^2/4m_x^2$. We note that $S_{H_1}^{g(\text{SM})} \simeq 0.651 + 0.050i$ for $M_{H_1} = 125.5$ GeV and $S_{H_2}^{g(\text{SM})} \simeq 0.291 + 0.744i$ for $M_{H_2} = 750$ GeV. In the limit $\tau \rightarrow 0$, $F_{sf}(0) = 2/3$. The mass of extra fermion F may be fixed by the relation $m_F = v_s g_{s\bar{F}F}^S + m_F^0$ where v_s denotes the VEV of the singlet s while m_F^0 is generated from a different origin other than v_s as in $-\mathcal{L}_{\text{mass}} \supset m_F^0 \bar{F}F$. We note that when $m_Q^0 = 0$, each contribution from a VLQ is not suppressed by $1/m_Q$ but by the common factor $1/v_s$.

Similarly, the couplings of $H_{1,2}$ to two photons are given by

$$\begin{aligned}
S_{H_1}^\gamma &= \cos \alpha S_{H_1}^{\gamma(\text{SM})} - \sin \alpha S_{H_1}^{\gamma(F)} \\
&\equiv \cos \alpha \left[2 \sum_{f=t,b,\tau} N_C Q_f^2 F_{sf}(\tau_{1f}) - F_1(\tau_{1W}) \right] - \sin \alpha \left[2 \sum_F N_C Q_F^2 g_{s\bar{F}F}^S \frac{v}{m_F} F_{sf}(\tau_{1F}) \right], \\
S_{H_2}^\gamma &= \sin \alpha S_{H_2}^{\gamma(\text{SM})} + \cos \alpha S_{H_2}^{\gamma(F)} \\
&\equiv \sin \alpha \left[2 \sum_{f=t,b,\tau} N_C Q_f^2 F_{sf}(\tau_{2f}) - F_1(\tau_{2W}) \right] + \cos \alpha \left[2 \sum_F N_C Q_F^2 g_{s\bar{F}F}^S \frac{v}{m_F} F_{sf}(\tau_{2F}) \right], \tag{6}
\end{aligned}$$

where $N_C = 3$ and 1 for quarks and leptons, respectively, and $Q_{f,F}$ denote the electric charges of fermions in the unit of e . In the limit $\tau \rightarrow 0$, $F_1(0) = 7$. We note that $S_{H_1}^{\gamma(\text{SM})} \simeq -6.55 + 0.039i$ for $M_{H_1} = 125.5$ GeV and $S_{H_2}^{\gamma(\text{SM})} \simeq -0.94 - 0.043i$ for $M_{H_2} = 750$ GeV.

B. Production and Decay

The production cross section of $H_{1,2}$ via the gluon-fusion process is given by

$$\sigma(gg \rightarrow H_{1,2}) = \frac{|S_{H_{1,2}}^g|^2}{|S_{H_{1,2}}^{g(\text{SM})}|^2} \sigma_{\text{SM}}(gg \rightarrow H_{1,2}) \tag{7}$$

with $\sigma_{\text{SM}}(gg \rightarrow H_1)$ and $\sigma_{\text{SM}}(gg \rightarrow H_2)$ denoting the corresponding SM cross sections for $M_{H_1} = 125.5$ GeV and $M_{H_2} = 750$ GeV, respectively. We note that $\sigma_{\text{SM}}(gg \rightarrow H_2) \approx 750$ fb at $\sqrt{s} = 13$ TeV.

The total decay widths of $H_{1,2}$ can be cast into the form

$$\begin{aligned}\Gamma_{H_1} &= \cos^2 \alpha \Gamma_{H_1}^{\text{SM}} + \Delta\Gamma_{\text{vis}}^{H_1 \rightarrow \gamma\gamma, gg, Z\gamma} + \Gamma_{H_1}^{\text{non-SM}}; \\ \Gamma_{H_2} &= \sin^2 \alpha \Gamma_{H_2}^{\text{SM}} + \Delta\Gamma_{\text{vis}}^{H_2 \rightarrow \gamma\gamma, gg, Z\gamma} + \Gamma_{H_2}^{\text{non-SM}},\end{aligned}\quad (8)$$

with $\Gamma_{H_1}^{\text{SM}} \simeq 4$ MeV and $\Gamma_{H_2}^{\text{SM}} \simeq 250$ GeV for the SM-like H_2 with $M_{H_2} = 750$ GeV[†]. And $\Gamma_{H_{1,2}}^{\text{non-SM}}$ denote additional partial decay widths of $H_{1,2}$ into non-SM particles which could be either visible or invisible. If the only non-SM particles into which $H_{1,2}$ can decay are invisible, one may have

$$\Gamma_{H_1}^{\text{non-SM}} = \Delta\Gamma_{\text{inv}}^{H_1}; \quad \Gamma_{H_2}^{\text{non-SM}} = \Gamma(H_2 \rightarrow H_1 H_1) + \Delta\Gamma_{\text{inv}}^{H_2}. \quad (9)$$

We note that $\Gamma_{H_2}^{\text{non-SM}}$ includes the H_2 decay into $H_1 H_1$ by definition. As we shall show that a sizeable $\Delta\Gamma_{\text{inv}}^{H_2}$ into invisible particles such as dark matters is required to accommodate a large $\Gamma_{H_2} = \mathcal{O}(10)$ GeV.

The quantities $\Delta\Gamma_{\text{vis}}^{H_{1,2} \rightarrow \gamma\gamma, gg}$ are given by

$$\begin{aligned}\Delta\Gamma_{\text{vis}}^{H_1 \rightarrow \gamma\gamma} &= \frac{M_{H_1}^3 \alpha^2}{256\pi^3 v^2} \left[|S_{H_1}^\gamma|^2 - \cos^2 \alpha |S_{H_1}^{\gamma(\text{SM})}|^2 \right], \\ \Delta\Gamma_{\text{vis}}^{H_1 \rightarrow gg} &= \left[1 + \frac{\alpha_s}{\pi} \left(\frac{95}{4} - 7 \right) \right] \frac{M_{H_1}^3 \alpha_s^2}{32\pi^3 v^2} \left[|S_{H_1}^g|^2 - \cos^2 \alpha |S_{H_1}^{g(\text{SM})}|^2 \right], \\ \Delta\Gamma_{\text{vis}}^{H_2 \rightarrow \gamma\gamma} &= \frac{M_{H_2}^3 \alpha^2}{256\pi^3 v^2} \left[|S_{H_2}^\gamma|^2 - \sin^2 \alpha |S_{H_2}^{\gamma(\text{SM})}|^2 \right], \\ \Delta\Gamma_{\text{vis}}^{H_2 \rightarrow gg} &= \left[1 + \frac{\alpha_s}{\pi} \left(\frac{95}{4} - 7 \right) \right] \frac{M_{H_2}^3 \alpha_s^2}{32\pi^3 v^2} \left[|S_{H_2}^g|^2 - \sin^2 \alpha |S_{H_2}^{g(\text{SM})}|^2 \right],\end{aligned}\quad (10)$$

with $\alpha_s = \alpha_s(M_{H_{1(2)}})$ for $\Delta\Gamma^{H_{1(2)} \rightarrow gg}$.

Before closing this section, we comment on the loop-induced decay widths $\Delta\Gamma_{\text{vis}}^{H_2 \rightarrow Z\gamma}$. The Higgs couplings are given by

$$S_{H_1}^{Z\gamma} = \cos \alpha S_{H_1}^{Z\gamma(\text{SM})} - \sin \alpha S_{H_1}^{Z\gamma(\text{F})}; \quad S_{H_2}^{Z\gamma} = \sin \alpha S_{H_2}^{Z\gamma(\text{SM})} + \cos \alpha S_{H_2}^{Z\gamma(\text{F})}, \quad (11)$$

[†] For $M_{H_2} = 750$ GeV, $\Gamma_{\text{SM}}(H_2 \rightarrow WW) \simeq 145$ GeV, $\Gamma_{\text{SM}}(H_2 \rightarrow ZZ) \simeq 71.9$ GeV, and $\Gamma_{\text{SM}}(H_2 \rightarrow t\bar{t}) \simeq 30.6$ GeV. [9].

with $S_{H_1}^{Z\gamma(\text{SM})} \simeq -11.042 + 0.010i$ and $S_{H_2}^{Z\gamma(\text{SM})} \simeq -0.0771 - 1.805i$. The contributions from VLFs are

$$S_{H_{1,2}}^{Z\gamma(\text{F})} = 2 \sum_F N_C Q_F \frac{2g_{Z\bar{F}F}}{s_W c_W} \left(g_{s\bar{F}F}^S \frac{v}{m_F} \right) m_F^2 F_f^{(0)}(M_{H_{1,2}}^2, m_F^2), \quad (12)$$

where Q_F and the couplings $g_{Z\bar{F}F}$ are defined in the interactions

$$-\mathcal{L} = Q_F e \bar{F} \gamma^\mu F A_\mu + \frac{e}{s_W c_W} g_{Z\bar{F}F} \bar{F} \gamma^\mu F Z_\mu,$$

and we note $2m_F^2 F_f^{(0)}(M_{H_{1,2}}^2, m_F^2) = F_{sf}(0) = 2/3$ in the heavy m_F limit, $m_F \rightarrow \infty$. Finally, the decay widths are given by

$$\begin{aligned} \Delta\Gamma_{\text{vis}}^{H_1 \rightarrow Z\gamma} &= \frac{M_{H_1}^3 \alpha^2}{128\pi^3 v^2} \left(1 - \frac{M_Z^2}{M_{H_1}^2} \right)^3 \left[|S_{H_1}^{Z\gamma}|^2 - \cos^2 \alpha |S_{H_1}^{Z\gamma(\text{SM})}|^2 \right], \\ \Delta\Gamma_{\text{vis}}^{H_2 \rightarrow Z\gamma} &= \frac{M_{H_2}^3 \alpha^2}{128\pi^3 v^2} \left(1 - \frac{M_Z^2}{M_{H_2}^2} \right)^3 \left[|S_{H_2}^{Z\gamma}|^2 - \sin^2 \alpha |S_{H_2}^{Z\gamma(\text{SM})}|^2 \right]. \end{aligned} \quad (13)$$

With no available independent information on the $g_{Z\bar{F}F}$ couplings, we neglect $\Delta\Gamma_{\text{vis}}^{H_{1,2} \rightarrow Z\gamma}$ by taking $g_{Z\bar{F}F} = 0$ when we perform global fits[‡].

III. HIGGS DATA

A. H_1 Data

For H_1 with $M_{H_1} = 125.5$ GeV, we use the signal strength data from Refs. [10, 11]. The theoretical signal strengths may be written as

$$\hat{\mu}(\mathcal{P}, \mathcal{D}) \simeq \hat{\mu}(\mathcal{P}) \hat{\mu}(\mathcal{D}), \quad (14)$$

where $\mathcal{P} = \text{ggF}, \text{VBF}, VH_1, ttH$ denote the H_1 production mechanisms: gluon fusion (ggF), vector-boson fusion (VBF), and associated productions with a $V = W/Z$ boson (VH_1) and top quarks (ttH_1) and $\mathcal{D} = \gamma\gamma, ZZ, WW, b\bar{b}, \tau\bar{\tau}$ the decay channels. Explicitly, we are taking

$$\begin{aligned} \hat{\mu}(\text{ggF}) &= |S_{H_1}^g|^2 / |S_{H_1}^{g(\text{SM})}|^2, \\ \hat{\mu}(\text{VBF}) &= \hat{\mu}(VH_1) = \hat{\mu}(ttH_1) = \cos^2 \alpha \end{aligned} \quad (15)$$

[‡] If $SU(2)$ symmetry is imposed onto the VLFs, the couplings of VLFs to photon and Z are correlated such that $g_{Z\bar{F}F}$ is given by $g_{Z\bar{F}F} = I_3^F - Q_F s_W^2$. See Section V for more discussions.

with $V = Z, W$. For the decay part,

$$\hat{\mu}(\mathcal{D}) = \frac{B(H_1 \rightarrow \mathcal{D})}{B(H_{\text{SM}} \rightarrow \mathcal{D})} \quad (16)$$

with

$$B(H_1 \rightarrow \gamma\gamma) = \frac{\Gamma(H_1 \rightarrow \gamma\gamma)}{\Gamma_{H_1}} = \frac{|S_{H_1}^\gamma|^2 / |S_{H_1}^{\gamma(\text{SM})}|^2 \Gamma(H_{\text{SM}} \rightarrow \gamma\gamma)}{\cos^2 \alpha \Gamma_{H_1}^{\text{SM}} + \Delta \Gamma_{\text{vis}}^{H_1 \rightarrow \gamma\gamma, gg, Z\gamma} + \Gamma_{H_1}^{\text{non-SM}}} \quad (17)$$

and

$$B(H_1 \rightarrow \mathcal{D}) = \frac{\Gamma(H_1 \rightarrow \mathcal{D})}{\Gamma_{H_1}} = \frac{\cos^2 \alpha \Gamma(H_{\text{SM}} \rightarrow \mathcal{D})}{\cos^2 \alpha \Gamma_{H_1}^{\text{SM}} + \Delta \Gamma_{\text{vis}}^{H_1 \rightarrow \gamma\gamma, gg, Z\gamma} + \Gamma_{H_1}^{\text{non-SM}}} \quad (18)$$

for $\mathcal{D} = ZZ, WW, b\bar{b}$ and $\tau\bar{\tau}$. If there are no VLF contributions to the H_1 couplings to photons and gluons or $S_{H_1}^{g(Q)} = S_{H_1}^{\gamma(F)} = 0$, the signal strengths are simply given by

$$\hat{\mu}(\mathcal{P}, \mathcal{D}) \simeq \frac{\cos^4 \alpha}{\cos^2 \alpha + \Gamma_{H_1}^{\text{non-SM}} / \Gamma_{H_1}^{\text{SM}}} . \quad (19)$$

For more details, we refer to Ref. [10].

B. H_2 Data

For H_2 with $M_{H_2} = 750$ GeV, we adopt the following cross sections for the diphoton process $pp \rightarrow H_2 \rightarrow \gamma\gamma$ measured at $\sqrt{s} = 13$ TeV [12, 13] in 2015:

$$\begin{aligned} \sigma^{\text{ATLAS}} &\approx 9.7 \pm 3.2 \text{ fb (for broad width) ,} \\ \sigma^{\text{ATLAS}} &\approx 6.3 \pm 2.4 \text{ fb (for narrow width) ,} \\ \sigma^{\text{CMS}} &\approx 6.3_{-3.1}^{+4.2} \text{ fb .} \end{aligned}$$

We also include the 8-TeV CMS data which correspond to the following cross section at $\sqrt{s} = 13$ TeV

$$\sigma^{\text{CMS}} \approx 3.5_{-1.8}^{+2.2} \text{ fb .}$$

In this work, we neglect the 8-TeV ATLAS data since they do not give positive-definite cross section at 1- σ level. We note that the ATLAS Collaboration gave the cross sections for the broad- and narrow-width cases separately. For definiteness we apply the broad-width value when $\Gamma_{H_2} \geq 40$ GeV and the narrow-width value when $\Gamma_{H_2} \leq 10$ GeV. However, we take the averaged value

$$\sigma^{\text{ATLAS}} \approx 8.0 \pm 2.8 \text{ fb}$$

TABLE I. The experimental values of the cross sections $\sigma(pp \rightarrow H_2 \rightarrow \gamma\gamma) \approx \sigma(pp \rightarrow H_2) \times B(H_2 \rightarrow \gamma\gamma)$ at $\sqrt{s} = 13$ GeV.

	13 TeV Data	8 TeV Data
ATLAS	6.3 ± 2.4 fb for $\Gamma_{H_2} \leq 10$ GeV	
	8.0 ± 2.8 fb for $10 \text{ GeV} < \Gamma_{H_2} < 40$ GeV	
	9.7 ± 3.2 fb for $\Gamma_{H_2} \geq 40$ GeV	
CMS	$6.3^{+4.2}_{-3.1}$ fb	$3.5^{+2.2}_{-1.8}$ fb

for intermediate Γ_{H_2} with $10 \text{ GeV} < \Gamma_{H_2} < 40 \text{ GeV}$. Strictly speaking, the CMS values are applicable only for the narrow-width case but, with no available data, we apply the same value for the intermediate- and broad-width cases too. Table I summarizes the experimental values of the cross sections $\sigma(pp \rightarrow H_2 \rightarrow \gamma\gamma)$ at $\sqrt{s} = 13$ GeV used in this work.

In this analysis, we further take into account the following experimental constraints on the H_2 production and its subsequent decays:

- Diboson: $\sigma(pp \rightarrow H_2)|_{\sqrt{s}=13 \text{ TeV}} \times B(H_2 \rightarrow VV) \lesssim 150$ fb [14]
- $t\bar{t}$: $\sigma(pp \rightarrow H_2)|_{\sqrt{s}=8 \text{ TeV}} \times B(H_2 \rightarrow t\bar{t}) \lesssim 0.5$ pb [15]
- Dijet: $\sigma(pp \rightarrow H_2)|_{\sqrt{s}=8 \text{ TeV}} \times B(H_2 \rightarrow gg) \lesssim 1$ pb [16].

We would like to comment on the constraint on $\Gamma(H_2 \rightarrow H_1 H_1)$ from the combined 95% upper limit on $\sigma(gg \rightarrow H_2) \times B(H_2 \rightarrow H_1 H_1) \lesssim 45$ fb at $\sqrt{s} = 8$ TeV [17]:

$$\Gamma(H_2 \rightarrow H_1 H_1) \lesssim 15 \text{ GeV} \left(\frac{150 \text{ fb}}{\sigma(gg \rightarrow H_2)} \right) \left(\frac{\Gamma_{H_2}}{50 \text{ GeV}} \right) \quad (20)$$

where we normalize the cross section $\sigma(gg \rightarrow H_2)$ using the corresponding SM Higgs production cross section for $M_{H_2} = 750$ GeV at $\sqrt{s} = 8$ TeV or $\sigma_{\text{SM}}(gg \rightarrow H_2)|_{\sqrt{s}=8 \text{ TeV}} \simeq 150$ fb which is smaller by a factor of 4.693 compared to $\sigma_{\text{SM}}(gg \rightarrow H_2)|_{\sqrt{s}=13 \text{ TeV}}$. If we parameterize the H_2 - H_1 - H_1 coupling as follows

$$\mathcal{L}_{3H} = g_{211} v H_2 H_1 H_1 \quad (21)$$

the constraint on $\Gamma(H_2 \rightarrow H_1 H_1)$ can be translated on the constraint on the coupling g_{211} :

$$\frac{g_{211}^2}{4\pi} \lesssim 0.4 \left(\frac{150 \text{ fb}}{\sigma(gg \rightarrow H_2)} \right) \left(\frac{\Gamma_{H_2}}{50 \text{ GeV}} \right) \quad (22)$$

using

$$\Gamma(H_2 \rightarrow H_1 H_1) = \frac{v^2 g_{211}^2}{8\pi M_{H_2}} \left(1 - \frac{4M_{H_1}^2}{M_{H_2}^2}\right)^{\frac{1}{2}}.$$

With a model-dependent coupling g_{211} , we do not impose any experimental constraint from $\sigma(gg \rightarrow H_2) \times B(H_2 \rightarrow H_1 H_1)$. Instead, as we shall see, we include $\Gamma(H_2 \rightarrow H_1 H_1)$ as a part of the free parameter which parameterizes non-SM decays of H_2 , as in $\Gamma_{H_2}^{\text{non-SM}} = \Gamma(H_2 \rightarrow H_1 H_1) + \Delta\Gamma_{\text{inv}}^{H_2}$, where the second term denotes additional partial decay widths of H_1 into invisible particles.

Finally, the vector-boson fusion (VBF) contribution to H_2 production is given by

$$\sigma^{\text{VBF}}(pp \rightarrow H_2 jj) = \sin^2 \alpha \sigma_{\text{SM}}^{\text{VBF}}(pp \rightarrow H_2 jj), \quad (23)$$

with $\sigma_{\text{SM}}^{\text{VBF}}(pp \rightarrow H_2 jj) \simeq 130$ fb with SM-like H_2 with mass 750 GeV at $\sqrt{s} = 13$ TeV [18]. While the gluon fusion process gives $\sigma(gg \rightarrow H_2) \sim 1250 \cos^2 \alpha |S_{H_2}^{g(Q)}|^2$ fb at $\sqrt{s} = 13$ TeV. With $\sin^2 \alpha \lesssim 0.2$, as will be seen, and a possibly large value of $|S_{H_2}^{g(Q)}| \sim \mathcal{O}(1)$, we can safely ignore the VBF production of H_2 in this work.

IV. FITS

In our approach, without loss of generality, we have the following 7 model-independent parameters:

$$\begin{aligned} & \sin \alpha ; \\ & S_{H_2}^{g(Q)}, \quad S_{H_2}^{\gamma(F)}, \quad \Gamma_{H_2}^{\text{non-SM}} ; \\ & S_{H_1}^{g(Q)}, \quad S_{H_1}^{\gamma(F)}, \quad \Gamma_{H_1}^{\text{non-SM}} . \end{aligned} \quad (24)$$

In our numerical analysis, we shall restrict ourselves to the case $2m_F > M_{H_2}$ so that $H_2 \rightarrow F\bar{F}$ decays are kinematically forbidden and $S_{H_1, H_2}^{g(Q), \gamma(F)}$ are all real. Furthermore, we note that

$$\begin{aligned} S_{H_1}^{g(Q)} &= \sum_Q g_{s\bar{Q}Q}^S \frac{v}{m_Q} F_{sf}(\tau_{1Q}) \simeq \frac{2}{3} \sum_Q g_{s\bar{Q}Q}^S \frac{v}{m_Q}, \\ S_{H_1}^{\gamma(F)} &= 2 \sum_F N_C Q_F^2 g_{s\bar{F}F}^S \frac{v}{m_F} F_{sf}(\tau_{1F}) \simeq \frac{4}{3} \sum_F N_C Q_F^2 g_{s\bar{F}F}^S \frac{v}{m_F}, \end{aligned} \quad (25)$$

since $F_{sf}(\tau_{1F}) \simeq F_{sf}(0) = 2/3$. This may imply $S_{H_1}^{g(Q), \gamma(F)}$ are not completely independent of $S_{H_2}^{g(Q), \gamma(F)}$. In the heavy m_F limit $m_F \rightarrow \infty$, for example, $F_{sf}(\tau_{1F}) = F_{sf}(\tau_{2F}) = F_{sf}(0) = 2/3$ and we have

$$S_{H_1}^{g(Q)} = S_{H_2}^{g(Q)}, \quad S_{H_1}^{\gamma(F)} = S_{H_2}^{\gamma(F)}. \quad (26)$$

On the other hand, if all the VLFs are degenerate around $m_F \sim M_{H_2}/2$ or $F_{sf}(\tau_{2F}) \simeq F_{sf}(1) = 1$ and we have

$$S_{H_1}^{g(Q)} = \frac{2}{3} S_{H_2}^{g(Q)} , \quad S_{H_1}^{\gamma(F)} = \frac{2}{3} S_{H_2}^{\gamma(F)} . \quad (27)$$

For convenience we introduce the parameters $\eta^{g(Q)}$ and $\eta^{\gamma(F)}$ are defined as in

$$S_{H_1}^{g(Q)} \equiv \eta^{g(Q)} S_{H_2}^{g(Q)} , \quad S_{H_1}^{\gamma(F)} \equiv \eta^{\gamma(F)} S_{H_2}^{\gamma(F)} . \quad (28)$$

We note that $|\eta^{g(Q)}|$ and $|\eta^{\gamma(F)}|$ take on values between $2/3$ and 1 if all the couplings $g_{s\bar{F}F}$ are either positive or negative, but in general can take on any values.

A. F4 fits

We first consider the minimal **F4** fit varying the following 4 parameters:

$$\sin \alpha ; \quad S_{H_2}^{g(Q)} , \quad S_{H_2}^{\gamma(F)} , \quad \Gamma_{H_2}^{\text{non-SM}} . \quad (29)$$

For the remaining parameters, first of all, we are taking $\Gamma_{H_1}^{\text{non-SM}} = 0$. For the η parameters, we consider the three extreme possibilities as follows:

- **F4-1** with $\eta^{g(Q)} = \eta^{\gamma(F)} = 0$: The VLFs are assumed not to contribute to the H_1 couplings to photons and gluons. In this case, the H_1 sector communicates with the H_2 sector only through the mixing angle $\sin \alpha$ and, accordingly, the signal strengths become $\hat{\mu}(\mathcal{P}, \mathcal{D}) \simeq \cos^2 \alpha$ independently of the production mechanism \mathcal{P} and the decay mode \mathcal{D}
- **F4-2** with $\eta^{g(Q)} = \eta^{\gamma(F)} = 2/3$: The VLFs are assumed to be almost degenerate with their masses around $M_{H_2}/2$.
- **F4-3** $\eta^{g(Q)} = \eta^{\gamma(F)} = 1$: All the VLFs are much heavier than H_2 .

And, the regions of the varying **F4**-fit parameters are taken as follows:

- $|\sin \alpha| \leq 0.5$: We consider the 95% confidence level (CL) limit of $\cos \alpha \gtrsim 0.86$ obtained from the global fits to Higgs-portal models using the current LHC H_1 data [6]. We shall show that $|\sin \alpha|$ would be more stringently constrained in the **F4-2** and **F4-3** fits with non-zero $\eta^{g(Q)}$ and $\eta^{\gamma(F)}$.

TABLE II. Best-fit values of **F4-1** with $\eta^{\gamma(F)} = \eta^{g(Q)} = 0$ and $\Gamma_{H_1}^{\text{non-SM}} = 0$, and varying: $\sin \alpha \in [-0.5 : 0.5]$, $S_{H_2}^{g(Q)} \in [-10 : 10]$, $S_{H_2}^{\gamma(F)} \in [-100 : 100]$, $\Gamma_{H_2}^{\text{non-SM}}/\text{GeV} \in [0 : 50]$. The decay widths are in units of GeV and the cross sections in units of fb. Other than the model parameters, the quantities shown are: Γ_{H_2} for the total decay width of H_2 , $C_{H_1}^{g,\gamma} \equiv |S_{H_1}^{g,\gamma}|/|S_{H_1}^{g(\text{SM}),\gamma(\text{SM})}|$, $\sigma(H_2) \equiv \sigma(gg \rightarrow H_2)$ at $\sqrt{s} = 13$ TeV, and $\sigma(XX) \equiv \sigma(gg \rightarrow H_2 \rightarrow XX) = \sigma(gg \rightarrow H_2) \times B(H_2 \rightarrow XX)$ at the same value of \sqrt{s} . The first line shows the best-fit values for the global minimum over the full range of Γ_{H_2} , whereas the second line shows the results for the broad-width case under the assumption of $\Gamma_{H_2} \geq 40$ GeV.

Fits	χ_{tot}^2	$\chi_{H_1}^2$	$\chi_{H_2}^2$	Best-fit values						
				$\sin \alpha$	$S_{H_2}^{\gamma(F)}$	$S_{H_2}^{g(Q)}$	$\Gamma_{H_1}^{\text{non-SM}}$	$\Gamma_{H_2}^{\text{non-SM}}$	$\eta^{\gamma(F)}$	$\eta^{g(Q)}$
F4-1	17.692	16.764	0.929	-4.6×10^{-4}	55.583	-0.299	0	3.012	0	0
	19.363	16.764	2.600	4.4×10^{-4}	-45.897	1.466	0	46.191	0	0

Best-fit values								
Γ_{H_2}	$C_{H_1}^\gamma$	$C_{H_1}^g$	$\sigma(H_2)$	$\sigma(\gamma\gamma)$	$\sigma(WW)$	$\sigma(ZZ)$	$\sigma(t\bar{t})$	$\sigma(gg)$
3.164	1.00	1.00	111.9	5.105	0.00	0.00	0.00	0.28
46.480	1.00	1.00	2693	5.696	0.00	0.00	0.00	11.05

- $|S_{H_2}^{g(Q)}| \leq 10$: We assume that $|S_{H_2}^{g(Q)}|$ cannot be larger than 10. In order to achieve the maximal value of $S_{H_2}^{g(Q)} \sim 10$, for example, there should be more than 20 VLQs with $m_Q \sim 500$ GeV and $g_{s\bar{Q}Q} \sim 1$. As we shall show, the H_2 dijet constraint gives $|S_{H_2}^{g(Q)}| \leq 7$.
- $|S_{H_2}^{\gamma(F)}| \leq 100$: We consider a 10 times larger region for $S_{H_2}^{\gamma(F)}$ compared to $S_{H_2}^{g(Q)}$ because of the possible enhancement factor $2N_C Q_F^2$ and additional contributions from VLLs to the H_2 couplings to photons.
- $\Gamma_{H_2}^{\text{non-SM}} \lesssim 50$ GeV: We restrict to the case in which the total width of H_2 does not exceed 50 GeV

TABLE III. The same as in TABLE II but with $\eta^{\gamma(F)} = \eta^{g(Q)} = 2/3$.

Fits	χ^2_{tot}	$\chi^2_{H_1}$	$\chi^2_{H_2}$	Best-fit values						
				$\sin \alpha$	$S_{H_2}^{\gamma(F)}$	$S_{H_2}^{g(Q)}$	$\Gamma_{H_1}^{\text{non-SM}}$	$\Gamma_{H_2}^{\text{non-SM}}$	$\eta^{\gamma(F)}$	$\eta^{g(Q)}$
F4-2	16.736	15.807	0.929	3.570×10^{-2}	29.400	0.329	0	0.777	2/3	2/3
	18.412	15.812	2.600	1.447×10^{-2}	74.395	0.893	0	45.55	2/3	2/3

Best-fit values								
Γ_{H_2}	$C_{H_1}^\gamma$	$C_{H_1}^g$	$\sigma(H_2)$	$\sigma(\gamma\gamma)$	$\sigma(WW)$	$\sigma(ZZ)$	$\sigma(t\bar{t})$	$\sigma(gg)$
1.146	1.105	0.987	144.9	5.085	20.83	10.21	4.84	1.30
45.93	1.108	0.987	1009	5.673	0.59	0.29	0.14	1.57

 TABLE IV. The same as in TABLE II but with $\eta^{\gamma(F)} = \eta^{g(Q)} = 1$.

Fits	χ^2_{tot}	$\chi^2_{H_1}$	$\chi^2_{H_2}$	Best-fit values						
				$\sin \alpha$	$S_{H_2}^{\gamma(F)}$	$S_{H_2}^{g(Q)}$	$\Gamma_{H_1}^{\text{non-SM}}$	$\Gamma_{H_2}^{\text{non-SM}}$	$\eta^{\gamma(F)}$	$\eta^{g(Q)}$
F4-3	16.740	15.810	0.929	-2.193×10^{-2}	-32.203	-0.396	0	1.753	1	1
	18.413	15.813	2.600	-0.933×10^{-2}	-75.915	-0.857	0	43.50	1	1

Best-fit values								
Γ_{H_2}	$C_{H_1}^\gamma$	$C_{H_1}^g$	$\sigma(H_2)$	$\sigma(\gamma\gamma)$	$\sigma(WW)$	$\sigma(ZZ)$	$\sigma(t\bar{t})$	$\sigma(gg)$
1.936	1.106	0.986	203.5	5.082	6.53	3.20	1.52	1.51
43.85	1.107	0.988	926.5	5.686	0.24	0.12	0.06	1.39

In Tables II, III, and IV, we show the best-fit values for the model parameters and miscellaneous quantities for the **F4-1**, **F4-2**, and **F4-3** fit, respectively. We first note that the global minima occur for the small value of $\Gamma_{H_2} = 1\text{-}3$ GeV though the larger widths are less preferred only by a small $\Delta\chi^2 < 2$. The broad-width minima under the assumption of $\Gamma_{H_2} > 40$ GeV give $\Gamma_{H_2} \sim 45$ GeV. The best-fit values of $\sin \alpha$ are either small or vanishingly small, independent of $\eta^{g(Q)}, \eta^{\gamma(F)}$.

The best-fit values for the cross section $\sigma(gg \rightarrow H_2 \rightarrow \gamma\gamma)$ are 5.1 fb and 5.7 fb, again independent of $\eta^{g(Q),\gamma(F)}$, for the global and broad-width minima, respectively. We find that

$$\sigma(gg \rightarrow H_2 \rightarrow \gamma\gamma) \simeq 0.06 \frac{(S_{H_2}^{g(Q)} S_{H_2}^{\gamma(F)})^2}{\Gamma_{H_2}/\text{GeV}} \text{ fb}. \quad (30)$$

Incidentally, we find

$$\sigma(gg \rightarrow H_2) \simeq 1250 (S_{H_2}^{g(Q)})^2 \text{ fb}, \quad (31)$$

and

$$\sigma(gg \rightarrow H_2 \rightarrow gg) \simeq 110 \frac{(S_{H_2}^{g(Q)})^4}{\Gamma_{H_2}/\text{GeV}} \text{ fb}. \quad (32)$$

For the **F4-2** and **F4-3** fits

$$\sigma(gg \rightarrow H_2 \rightarrow WW) \simeq 16.5 \times 10^4 \frac{(S_{H_2}^{g(Q)})^2 \sin^2 \alpha}{\Gamma_{H_2}/\text{GeV}} \text{ fb}, \quad (33)$$

and $\sigma(gg \rightarrow H_2 \rightarrow ZZ) \sim \sigma(gg \rightarrow H_2 \rightarrow WW)/2$ and $\sigma(gg \rightarrow H_2 \rightarrow t\bar{t}) \sim \sigma(gg \rightarrow H_2 \rightarrow WW)/4$.[§] Finally,

$$\begin{aligned} C_{H_1}^\gamma &= \left| \frac{S_{H_1}^\gamma}{S_{H_1}^{\gamma(\text{SM})}} \right| \simeq \left| 1 + \sin \alpha \frac{\eta^{\gamma(F)} S_{H_2}^{\gamma(F)}}{6.55} \right|, \\ C_{H_1}^g &= \left| \frac{S_{H_1}^g}{S_{H_1}^{g(\text{SM})}} \right| \simeq \left| 1 - \sin \alpha \frac{\eta^{g(Q)} S_{H_2}^{g(Q)}}{0.653} \right|. \end{aligned} \quad (34)$$

Figure 1 shows $\Delta\chi^2$ vs $\sin \alpha$ for the **F4-1** (left), **F4-2** (middle), and **F4-3** (right) fits. The upper frames show the results over the full range of Γ_{H_2} , while the lower frames show the results for the broad-width case under the assumption of $\Gamma_{H_2} \geq 40$ GeV. The regions shown are for $\Delta\chi^2 = 2.3$ (red), 5.99 (green), and 11.83 (blue) above the minimum and the triangles denote the corresponding minima. First of all, we note that the minima occur at $\sin \alpha \sim 0$ in all the cases. Also, since $\Gamma_{H_2} \geq \sin^2 \alpha \Gamma_{H_2}^{\text{SM}}$, we observe

$$\sin^2 \alpha \leq \frac{\Gamma_{H_2}}{\Gamma_{H_2}^{\text{SM}}} \quad (35)$$

which implies, for example, $|\sin \alpha| \lesssim 0.2$ (0.4) when $\Gamma_{H_2} \lesssim 10$ (40) GeV and $|\sin \alpha|$ cannot exceed ~ 0.45 if $\Gamma_{H_2} \leq 50$ GeV. In the **F4-1** fits, as shown in Table II, the minimum for the

[§] Here we have assumed that the VLFs are singlet and thus do not couple directly to W bosons. However, if the VLFs are arranged into $SU(2)$ doublets, the VLFs can couple directly to W bosons and thus contributing to the $H_2 \rightarrow WW$ decay via loops. See Section V for more discussions.

full range of Γ_{H_2} is deeper than that for the broad-width case. From the upper-left frame of Fig. 1, $|\sin \alpha| \lesssim 0.2$ in the $\Delta\chi^2 \lesssim 1$ region and we find $\Gamma_{H_2} \lesssim 10$ GeV there. In the **F4-2** and **F4-3** fits, in addition to the global minima at $\sin \alpha \sim 0$, two more local minima are developed at non-zero $\sin \alpha$. The local minima are developed at $|\sin \alpha| \simeq 0.20$ (0.13) for the **F4-2** (**F4-3**) fits when $S_{H_1}^\gamma = -S_{H_1}^{\gamma(\text{SM})}$ and $|S_{H_1}^{\gamma(F)}| \simeq 100$, as we shall show soon.

In Fig. 2 we show $\Delta\chi^2$ vs $\Gamma_{H_2}^{\text{non-SM}}$ for the **F4-1** (left), **F4-2** (middle), and **F4-3** (right) fits. Again, the upper frames are for the full range of Γ_{H_2} while the lower ones for the broad-width case with $\Gamma_{H_2} \geq 40$ GeV. We do not see any dependence on $\eta^{g(Q),\gamma(F)}$ in the upper frames since the H_2 width does not depend on them. The narrow width values are slightly preferred and $\Delta\chi^2 = 0$ is possible only when $\Gamma_{H_2}^{\text{non-SM}} \lesssim 10$ GeV. This is because the ATLAS data on $\sigma(pp \rightarrow H_2 \rightarrow \gamma\gamma)$ are closer to the CMS data when $\Gamma_{H_2} \leq 10$ GeV, see Table I. In the lower frames, we observe that, in the $\Delta\chi^2 \leq 2.3$ region (red), $\Gamma_{H_2}^{\text{non-SM}} \gtrsim 12$ GeV, 36 GeV, and 36 GeV to achieve $\Gamma_{H_2} \geq 40$ GeV for $\eta^{g(Q),\gamma(F)} = 0$ (**F4-1**, left), $\eta^{g(Q),\gamma(F)} = 2/3$ (**F4-2**, middle), and $\eta^{g(Q),\gamma(F)} = 1$ (**F4-3**, right), respectively.

Figure 3 shows the CL regions in the $(\sin \alpha, S_{H_2}^{g(Q)})$ plane. When $\sin \alpha \sim 0$, $|S_{H_2}^{g(Q)}|$ is mostly constrained by $\sigma(pp \rightarrow H_2)|_{\sqrt{s}=8\text{ TeV}} \times B(H_2 \rightarrow gg) \lesssim 1$ pb. Using Eq. (32) and $\sigma(gg \rightarrow H_2)|_{\sqrt{s}=8\text{ TeV}} = \sigma(gg \rightarrow H_2)|_{\sqrt{s}=13\text{ TeV}}/4.7$, one may have $|S_{H_2}^{g(Q)}| \lesssim 7 (\Gamma_{H_2}/50\text{ GeV})^{1/4}$. As $\sin \alpha$ deviates from 0, $|S_{H_2}^{g(Q)}|$ becomes constrained by $\sigma(pp \rightarrow H_2)|_{\sqrt{s}=13\text{ TeV}} \times B(H_2 \rightarrow VV) \lesssim 150$ fb. Using Eq. (33), one may have $|S_{H_2}^{g(Q)} \sin \alpha| \lesssim 0.2 (\Gamma_{H_2}/50\text{ GeV})^{1/2}$. These two observations mainly explain the shape of the CL regions in the left frames for **F4-1** with $\eta^{g(Q),\gamma(F)} = 0$. For **F4-2** and **F4-3** with $\eta^{g(Q),\gamma(F)} \neq 1$, the H_1 data provide additional constraints basically coming from $C_{H_1}^{g,\gamma} \sim 1$. Definitely, the CL regions populate along the $\sin \alpha = 0$ line satisfying the H_1 constraints in the case $(S_{H_1}^\gamma, S_{H_1}^g) \sim (+S_{H_1}^{\gamma(\text{SM})}, +S_{H_1}^{g(\text{SM})})$. On the other hand, the four islands around the points $(|\sin \alpha| = 0.20, |S_{H_2}^{g(Q)}| = 0.5)$ and $(|\sin \alpha| = 0.13, |S_{H_2}^{g(Q)}| = 0.5)$ for the **F4-2** and **F4-3** fits, respectively, satisfy the H_1 constraints in the case $(S_{H_1}^\gamma, S_{H_1}^g) \sim (-S_{H_1}^{\gamma(\text{SM})}, +S_{H_1}^{g(\text{SM})})$. We find that the cases with $S_{H_1}^g \sim -S_{H_1}^{g(\text{SM})}$ cannot satisfy the H_1 constraints because it requires a too large value of $|S_{H_2}^{g(Q)}| \sim 10$ ¶ which is incompatible with the H_2 dijet constraint $|S_{H_2}^{g(Q)}| \lesssim 7$ discussed before. Some numerical results on 68% CL regions are summarized in Table V.

¶ Note that the relation $S_{H_1}^g \sim -S_{H_1}^{g(\text{SM})}$ leads to $\sin \alpha S_{H_1}^{g(Q)} = \sin \alpha \eta^{g(Q)} S_{H_2}^{g(Q)} \sim (1 + \cos \alpha) S_{H_1}^{g(\text{SM})} \simeq 1.3$.

For $|\sin \alpha| = 0.20$ (0.13) and $\eta^{g(Q)} = 2/3$ (1), one may have $|S_{H_2}^{g(Q)}| \sim 10$.

TABLE V. The 68% CL regions of $\sigma(\gamma\gamma) = \sigma(gg \rightarrow H_2) \times B(H_2 \rightarrow \gamma\gamma)$, $\sin \alpha$, $\Gamma_{H_2}^{\text{non-SM}}/\text{GeV}$, $S_{H_2}^{g(Q)}$, and $S_{H_2}^{\gamma(F)}$ in the **F4** fits.

Fits	$\eta^{g(Q),\gamma(F)}$	Γ_{H_2}/GeV	$\sigma(\gamma\gamma)/\text{fb}$	$ \sin \alpha $	$\Gamma_{H_2}^{\text{non-SM}}$	$ S_{H_2}^{g(Q)} $	$ S_{H_2}^{\gamma(F)} $
F4-1	0	0~50	2.9~7.4	0~0.33	0~50	0.05~7.0	2.2~100
	0	40~50	3.3~8.2	0~0.34	12~50	0.4~7.0	7.2~100
F4-2	2/3	0~50	2.9~7.4	0~0.095 or 0.20~0.24	0~50	0.05~6.6	2.4~100
	2/3	40~50	3.3~8.2	0~0.066	36~50	0.5~7.0	7.9~100
F4-3	1	0~50	2.9~7.4	0~0.077 or 0.13~0.20	0~50	0.05~6.6	2.4~100
	1	40~50	3.3~8.2	0~0.044	36~50	0.5~7.0	7.9~100

Figure 4 shows the CL regions in the $(\sin \alpha, S_{H_2}^{\gamma(F)})$ plane. For **F4-1** with $\eta^{g(Q),\gamma(F)} = 0$, the parameter space is constrained basically by the lower limit on $\sigma(gg \rightarrow H_2 \rightarrow \gamma\gamma)$. The lower limit $\sigma_{\min} \sim 3$ fb in at 68% CL, see Table V. Then, using Eq. (30), we have $|S_{H_2}^{g(Q)} S_{H_2}^{\gamma(F)}| \gtrsim 50 (\Gamma_{H_2}/50 \text{ GeV})^{1/2} (\sigma_{\min}/3\text{fb})^{1/2}$. Combining this with the the H_2 diboson constraint $|S_{H_2}^{g(Q)} \sin \alpha| \lesssim 0.2 (\Gamma_{H_2}/50 \text{ GeV})^{1/2}$, we obtain $|S_{H_2}^{\gamma(F)}| \gtrsim 250 |\sin \alpha| (\sigma_{\min}/3\text{fb})^{1/2}$. This observation basically explains the shape of CL regions in the left frames together with the fact that the lower limit σ_{\min} increases a little bit as $|\sin \alpha|$ deviates from 0, see Fig. 5. For **F4-2** and **4-3** with $\eta^{g(Q),\gamma(F)} \neq 0$, on the other hand, the H_1 data gives further constraints like as in the $(\sin \alpha, S_{H_2}^{g(Q)})$ case. In the CL regions along the $\sin \alpha = 0$ line, $(S_{H_1}^{\gamma}, S_{H_1}^g) \sim (+S_{H_1}^{\gamma(\text{SM})}, +S_{H_1}^{g(\text{SM})})$. While, on the two islands at non-zero $\sin \alpha$ and for large values of $|S_{H_2}^{\gamma(F)}|$, $(S_{H_1}^{\gamma}, S_{H_1}^g) \sim (-S_{H_1}^{\gamma(\text{SM})}, +S_{H_1}^{g(\text{SM})})$. When $S_{H_1}^{\gamma} = -S_{H_1}^{\gamma(\text{SM})}$, we have

$$\sin \alpha S_{H_1}^{\gamma(F)} = \sin \alpha \eta^{\gamma(F)} S_{H_2}^{\gamma(F)} = (1 + \cos \alpha) S_{H_1}^{\gamma(\text{SM})} \simeq -13, \quad (36)$$

which implies that the local minima appear at $\sin \alpha \simeq -13/(\eta^{\gamma(F)} S_{H_2}^{\gamma(F)})$. When $S_{H_2}^{\gamma(F)} = \pm 100$, for example, the local minima may occur at $\sin \alpha \simeq \mp 0.20$ and ∓ 0.13 for the **F4-2** ($\eta^{\gamma(F)} = 2/3$) and the **F4-3** ($\eta^{\gamma(F)} = 1$), respectively. This finally explains why the local minima are developed at $|\sin \alpha| \simeq 0.20$ (0.13) in the middle (right) frames of Fig. 1.

Figure 5 shows the CL regions in the $(\sin \alpha, \sigma(gg \rightarrow H_2) \times B(H_2 \rightarrow \gamma\gamma))$ plane. We observe the cross sections are centered around 5 fb.

Figure 6 shows the CL regions in the $(\sin \alpha, \sigma(gg \rightarrow H_2) \times B(H_2 \rightarrow gg))$ plane. The cross section can be as large as up to 5 pb around $\sin \alpha = 0$, limited by the current H_2 dijet constraint.

Figure 7 shows the CL regions in the $(\sin \alpha, \sigma(gg \rightarrow H_2) \times B(H_2 \rightarrow WW))$ plane. As $\sin \alpha$ deviates from 0, the cross section can be as large as 150 fb, limited by the current H_2 diboson constraint.

Compared to $\sigma(gg \rightarrow H_2) \times B(H_2 \rightarrow WW)$, the cross sections $\sigma(gg \rightarrow H_2) \times B(H_2 \rightarrow ZZ)$ and $\sigma(gg \rightarrow H_2) \times B(H_2 \rightarrow t\bar{t})$ can be as large as 70 fb and 36 fb, respectively, suppressed by the factors $B(H_2 \rightarrow ZZ)/B(H_2 \rightarrow WW) \sim 1/2$ and $B(H_2 \rightarrow t\bar{t})/B(H_2 \rightarrow WW) \sim 1/5$: see FIGs. 8 and 9. Otherwise, their patterns are similar.

Finally, in FIG. 10, we show the CL regions in the $(\Gamma_{H_2}, (\Delta B_{\text{inv}}^{H_2})_{\text{min}})$ plane where

$$(\Delta B_{\text{inv}}^{H_2})_{\text{min}} \equiv \frac{(\Delta \Gamma_{\text{inv}}^{H_2})_{\text{min}}}{\Gamma_{H_2}}$$

denoting the minimum value of the H_2 branching ratio into invisible particles. The minimum invisible decay width is obtained by requiring the decay width $\Gamma(H_2 \rightarrow H_1 H_1)$ to saturate the current upper limit on $\sigma(gg \rightarrow H_2) \times B(H_2 \rightarrow H_1 H_2)$. More explicitly, we have

$$(\Delta \Gamma_{\text{inv}}^{H_2})_{\text{min}} = \Gamma_{H_2} - \left[\sin^2 \alpha \Gamma_{H_2}^{\text{SM}} + \Delta \Gamma_{\text{vis}}^{H_2 \rightarrow \gamma\gamma} + \Delta \Gamma_{\text{vis}}^{H_2 \rightarrow gg} + \Gamma(H_2 \rightarrow H_1 H_1)_{\text{max}} \right] \quad (37)$$

with

$$\Gamma(H_2 \rightarrow H_1 H_1)_{\text{max}} = 15 \text{ GeV} \left(\frac{150 \text{ fb}}{\sigma(gg \rightarrow H_2)|_{\sqrt{s}=8 \text{ TeV}}} \right) \left(\frac{\Gamma_{H_2}}{50 \text{ GeV}} \right) \quad (38)$$

where we again take $\sigma(gg \rightarrow H_2)|_{\sqrt{s}=8 \text{ TeV}} = \sigma(gg \rightarrow H_2)|_{\sqrt{s}=13 \text{ TeV}}/4.7$, see Eq. (20). We observe that, at 68% CL, $(\Delta B_{\text{inv}}^{H_2})_{\text{min}} \sim 0$ can accommodate the situation with $\Gamma_{H_2} \lesssim 40 (32, 32) \text{ GeV}$ for **F4-1** (**F4-2**, **F4-3**). But it should be larger than ~ 0.2 in order to accommodate the value $\Gamma_{H_2} \gtrsim 40 \text{ GeV}$. Especially, when $\Gamma_{H_2} \sim 50 \text{ GeV}$, the invisible branching ratio should be larger than 0.3, 0.45, and 0.45 for **F4-1**, **F4-2**, and **F4-3**, respectively, at 68% CL.

V. $H_2 \rightarrow WW, ZZ, Z\gamma$

In this section, we consider the more general case in which there exist interactions between VLQs and W/Z bosons. Then, even in the limit of $\sin \alpha = 0$, H_2 can decay into WW and ZZ via VLQ loops and, more importantly, into $Z\gamma$.

Note that the couplings of VLQs to W/Z bosons are highly model dependent on the weak isospin and the $U(1)_Y$ hypercharges. In order to be specific but without much loss of generality, we introduce N_d copies of VLQ doublets $Q_d = (U, D)^T$ and N_s copies of VLQ singlets Q_s which couples to the SM gauge bosons as follows:

$$\begin{aligned} -\mathcal{L}_{\text{QCD}} &= g_s \left(\bar{U} \gamma^\mu T^a U + \bar{D} \gamma^\mu T^a D + \bar{Q}_s \gamma^\mu T^a Q_s \right) G_\mu^a, \\ -\mathcal{L}_{\text{EW}} &= \bar{Q}_d \gamma^\mu \left(g \frac{\tau^a}{2} W_\mu^a + g' \frac{Y_d}{2} B_\mu \right) Q_d + \bar{Q}_s \gamma^\mu \left(g' \frac{Y_s}{2} B_\mu \right) Q_s, \end{aligned} \quad (39)$$

where g_s denotes the $SU(3)$ gauge coupling, $g = e/s_W$ and $g' = e/c_W = gt_W$ with $s_W \equiv \sin \theta_W$, $c_W \equiv \cos \theta_W$, and $t_W = s_W/c_W$, and T^a and $\tau^a/2$ are generators of $SU(3)$ and $SU(2)$ groups. And Y_d and Y_s denote the $U(1)_Y$ hypercharges of doublet Q_d and singlet Q_s , respectively. They are related with the electric charges of VLQs by:

$$Q_{Q_s} = Y_s/2, \quad Q_U = 1/2 + Y_d/2, \quad Q_D = -1/2 + Y_d/2. \quad (40)$$

Note that $Q_U - Q_D = 1$ independently of Y_d . After rotating $(W_\mu^3, B_\mu)^T$ into $(Z_\mu, A_\mu)^T$ as usual or replacing W_μ^3 and B_μ with $c_W Z_\mu + s_W A_\mu$ and $-s_W Z_\mu + c_W A_\mu$, respectively, one may have

$$\begin{aligned} -\mathcal{L}_{\text{EW}} &= e \left[Q_U \bar{U} \gamma^\mu U + Q_D \bar{D} \gamma^\mu D + Q_{Q_s} \bar{Q}_s \gamma^\mu Q_s \right] A_\mu \\ &+ \frac{g}{c_W} \left[\bar{U} \gamma^\mu U \left(\frac{1}{2} - s_W^2 Q_U \right) + \bar{D} \gamma^\mu D \left(-\frac{1}{2} - s_W^2 Q_D \right) + \bar{Q}_s \gamma^\mu Q_s \left(-s_W^2 Q_{Q_s} \right) \right] Z_\mu \\ &+ \frac{g}{\sqrt{2}} (\bar{U} \gamma^\mu D W_\mu^+ + \bar{D} \gamma^\mu U W_\mu^-). \end{aligned} \quad (41)$$

We note the couplings to the Z boson are purely vector-like and proportional to the factors $\pm 1/2 - s_W^2 Q_{U,D}$ which are different from the SM case where only the left-handed quarks are participating in the $SU(2)$ interaction. Further we note that the couplings to the Z boson become the same as those to photons taking $(I_3^F - s_W^2 Q_F)/s_W c_W \rightarrow Q_F$ with $I_3^U = -I_3^D = 1/2$ and $I_3^{Q_s} = 0$. Incidentally, the Yukawa couplings of VLQs to the singlet s are given by

$$-\mathcal{L}_Y = g_{s\bar{Q}_d Q_d}^S s \bar{Q}_d Q_d + g_{s\bar{Q}_s Q_s}^S s \bar{Q}_s Q_s. \quad (42)$$

With all these couplings given, one can calculate the VLQ-loop contributions to the H_2 couplings to gg , $\gamma\gamma$, $Z\gamma$, ZZ , and WW , which are proportional to $\cos \alpha$. For the H_2

couplings to two gluons and two photons, adopting the same notations as in Eqs. (5) and (6), we have

$$S_{H_2}^{g(Q)} = \sum_{Q_d} g_{s\bar{Q}_d Q_d}^S \left[\frac{v}{m_U} F_{sf}(\tau_{2U}) + \frac{v}{m_D} F_{sf}(\tau_{2D}) \right] + \sum_{Q_s} g_{s\bar{Q}_s Q_s}^S \frac{v}{m_{Q_s}} F_{sf}(\tau_{2Q_s}) , \quad (43)$$

$$S_{H_2}^{\gamma(F)} = 2 \sum_{Q_d} N_C g_{s\bar{Q}_d Q_d}^S \left[Q_U^2 \frac{v}{m_U} F_{sf}(\tau_{2U}) + Q_D^2 \frac{v}{m_D} F_{sf}(\tau_{2D}) \right] + 2 \sum_{Q_s} N_C g_{s\bar{Q}_s Q_s}^S Q_{Q_s}^2 \frac{v}{m_{Q_s}} F_{sf}(\tau_{2Q_s}) .$$

On the other hand, for the H_2 coupling to Z and γ , following the convention of Eq. (11), we have

$$\begin{aligned} S_{H_2}^{Z\gamma(F)} = & 2 \sum_{Q_d} N_C g_{s\bar{Q}_d Q_d}^S \left\{ Q_U \frac{(1/2 - s_W^2 Q_U)}{s_W c_W} \frac{v}{m_U} \left[2m_U^2 F_f^{(0)}(M_{H_2}^2, m_U^2) \right] \right. \\ & \left. + Q_D \frac{(-1/2 - s_W^2 Q_D)}{s_W c_W} \frac{v}{m_D} \left[2m_D^2 F_f^{(0)}(M_{H_2}^2, m_D^2) \right] \right\} \\ & + 2 \sum_{Q_s} N_C g_{s\bar{Q}_s Q_s}^S \left\{ Q_{Q_s} \frac{(-s_W^2 Q_{Q_s})}{s_W c_W} \frac{v}{m_{Q_s}} \left[2m_{Q_s}^2 F_f^{(0)}(M_{H_2}^2, m_{Q_s}^2) \right] \right\} . \end{aligned} \quad (44)$$

Note that, in the limit of $M_Z = 0$, we have $2m_X^2 F_f^{(0)}(M_{H_2}^2, m_X^2) = F_{sf}(\tau_{2X})$ leading to $S_{H_2}^{Z\gamma(F)} = S_{H_2}^{\gamma(F)}$ after replacing $(I_3^F - s_W^2 Q_F)/s_W c_W$ with Q_F as noted following Eq. (41).

For the decay processes $H_2 \rightarrow VV$ with $V = W/Z$, the amplitude is given by

$$\mathcal{M}_{VVH_2} = \sin \alpha \mathcal{M}_{VVH_2}^{(0)} + \cos \alpha \mathcal{M}_{VVH_2}^{(1)} \quad (45)$$

and, in the leading order neglecting the SM one-loop contributions to the hWW vertex, the tree-level and one-loop amplitudes are

$$\begin{aligned} \mathcal{M}_{WWH_2}^{(0)} &= -g M_W \epsilon_1^* \cdot \epsilon_2^* , \\ \mathcal{M}_{ZZH_2}^{(0)} &= -\frac{g M_W}{c_W^2} \epsilon_1^* \cdot \epsilon_2^* , \\ \mathcal{M}_{VVH_2}^{(1)} &= -\frac{\alpha}{2\pi v} S_{H_2}^{VV(F)} [k_1 \cdot k_2 \epsilon_1^* \cdot \epsilon_2^* - k_1 \cdot \epsilon_2^* k_2 \cdot \epsilon_1^*] , \end{aligned} \quad (46)$$

where $k_{1,2}$ are the momenta of the two massive vector bosons with $2k_1 \cdot k_2 = M_{H_2}^2 - 2M_V^2$ and $\epsilon_{1,2}$ are their polarization vectors. Note that there exists a tree-level contribution to the amplitude when $\sin \alpha \neq 0$ which has different vertex structure from the loop-induced one.

The form factor $S_{H_2}^{ZZ(F)}$ can be cast into the form

$$S_{H_2}^{ZZ(F)} = 2 \sum_{Q_d} N_C g_{s\bar{Q}_d Q_d}^S \left\{ \frac{(1/2 - s_W^2 Q_U)^2}{s_W^2 c_W^2} \frac{v}{m_U} \left[2m_U^2 F_f^{(1)}(M_{H_2}^2, m_U^2) \right] \right.$$

$$\begin{aligned}
& + \frac{(-1/2 - s_W^2 Q_D)^2}{s_W^2 c_W^2} \frac{v}{m_D} \left[2m_D^2 F_f^{(1)}(M_{H_2}^2, m_D^2) \right] \Big\} \\
& + 2 \sum_{Q_s} N_C g_{s\bar{Q}_s Q_s}^S \frac{(-s_W^2 Q_{Q_s})^2}{s_W^2 c_W^2} \frac{v}{m_{Q_s}} \left[2m_{Q_s}^2 F_f^{(1)}(M_{H_2}^2, m_{Q_s}^2) \right] . \tag{47}
\end{aligned}$$

Note that, in the limit of $M_Z = 0$, we have $2m_X^2 F_f^{(1)}(M_{H_2}^2, m_X^2) = F_{sf}(\tau_{2X})$ leading to $S_{H_2}^{ZZ(F)} = S_{H_2}^{\gamma(F)}$ after replacing $(I_3^F - s_W^2 Q_F)/s_W c_W$ with Q_F , see Eq. (41).

Similarly, $S_{H_2}^{WW(F)}$ may take the form

$$S_{H_2}^{WW(F)} = 2 \sum_{Q_d} N_C g_{s\bar{Q}_d Q_d}^S \frac{1}{2s_W^2} \frac{v}{m_{Q_d}} \left[2m_{Q_d}^2 F_f^{(2)}(M_{H_2}^2, m_{Q_d}^2) \right] , \tag{48}$$

in the limit of $m_U = m_D = m_{Q_d}$. Also note that, in the limit of $M_W = 0$, $2m_{Q_d}^2 F_f^{(2)}(M_{H_2}^2, m_{Q_d}^2) = F_{sf}(\tau_{2Q_d})$ and $S_{H_2}^{WW(F)}$ becomes the same as the singlet contribution to $S_{H_2}^{\gamma(F)}$ after replacing $1/\sqrt{2}s_W$ with Q_{Q_s} and, subsequently, Q_d with Q_s .

In the previous section, we are taking $S_{H_2}^{\gamma(F)}$ and $S_{H_2}^{g(Q)}$ as our independent fitting parameters. In general, the form factors $S_{H_2}^{Z\gamma(F)}$, $S_{H_2}^{ZZ(F)}$, and $S_{H_2}^{WW(F)}$ are independent of $S_{H_2}^{\gamma(F)}$ and $S_{H_2}^{g(Q)}$ and they should be treated as independent parameters. But we find that they can be expressed in terms of $S_{H_2}^{\gamma(F)}$ and $S_{H_2}^{g(Q)}$ when

$$\frac{M_{Z,W}}{M_{H_2}} \rightarrow 0, \quad g_{s\bar{Q}_d Q_d}^S = g_{s\bar{Q}_s Q_s}^S, \quad m_U = m_D = m_{Q_s} . \tag{49}$$

In the above limit, we have

$$\begin{aligned}
S_{H_2}^{Z\gamma(F)} &= -t_W S_{H_2}^{\gamma(F)} + \left(\frac{N_d}{2N_d + N_s} \right) \frac{N_C}{s_W c_W} S_{H_2}^{g(Q)} , \\
S_{H_2}^{ZZ(F)} &= t_W^2 S_{H_2}^{\gamma(F)} + \left(\frac{N_d}{2N_d + N_s} \right) \frac{1 - 2s_W^2}{s_W^2 c_W^2} N_C S_{H_2}^{g(Q)} , \\
S_{H_2}^{WW(F)} &= \left(\frac{N_d}{2N_d + N_s} \right) \frac{N_C}{s_W^2} S_{H_2}^{g(Q)} , \tag{50}
\end{aligned}$$

where we use $Q_U - Q_D = 1$. Note that the form factors $S_{H_2}^{Z\gamma(F)}$, $S_{H_2}^{ZZ(F)}$, and $S_{H_2}^{WW(F)}$ are all fixed once $S_{H_2}^{\gamma(F)}$, $S_{H_2}^{g(Q)}$, N_d , and N_s are given and, accordingly, one can calculate the decay widths of H_2 into $Z\gamma$, ZZ , and WW , see Appendix A.

In Fig. 11, we shows the CL regions in the $(\sin \alpha, \sigma(gg \rightarrow H_2) \times B(H_2 \rightarrow WW))$ plane including the VLQ-loop induced contributions to $B(H_2 \rightarrow WW)$ in the presence of interactions between VLQs and W/Z bosons. We are taking the limits suggested in Eq. (49) and

$N_d = N_s$. Compared to Figure 7, we observe that there are non-vanishing VLF contributions to $\sigma(gg \rightarrow H_2) \times B(H_2 \rightarrow WW)$ when $\sin \alpha \rightarrow 0$ because:

$$\Gamma(H_2 \rightarrow WW)|_{\sin \alpha \rightarrow 0} \simeq \frac{M_{H_2}^3 \alpha^2}{128 \pi^3 v^2} (S_{H_2}^{WW(F)})^2 = \frac{M_{H_2}^3 \alpha^2}{128 \pi^3 v^2} \frac{(S_{H_2}^{g(Q)})^2}{s_W^4}. \quad (51)$$

Figure 12 shows the CL regions in the $(\sin \alpha, \sigma(gg \rightarrow H_2) \times B(H_2 \rightarrow ZZ))$ plane in the same context. Compared to Figure 8, we observe that there are also non-vanishing VLF contributions when $\sin \alpha \rightarrow 0$ because:

$$\Gamma(H_2 \rightarrow ZZ)|_{\sin \alpha \rightarrow 0} \simeq \frac{M_{H_2}^3 \alpha^2}{256 \pi^3 v^2} (S_{H_2}^{ZZ(F)})^2 = \frac{M_{H_2}^3 \alpha^2}{256 \pi^3 v^2} \left(t_W^2 S_{H_2}^{\gamma(F)} + \frac{1 - 2s_W^2}{s_W^2 c_W^2} S_{H_2}^{g(Q)} \right)^2. \quad (52)$$

Figure 13 shows the CL regions in the $(\sin \alpha, \sigma(gg \rightarrow H_2) \times B(H_2 \rightarrow Z\gamma))$ plane. In the limits suggested in Eq. (49) with $N_d = N_s$, we have

$$\Gamma(H_2 \rightarrow Z\gamma)|_{\sin \alpha \rightarrow 0} \simeq \frac{M_{H_2}^3 \alpha^2}{128 \pi^3 v^2} (S_{H_2}^{Z\gamma(F)})^2 = \frac{M_{H_2}^3 \alpha^2}{128 \pi^3 v^2} \left(-t_W S_{H_2}^{\gamma(F)} + \frac{S_{H_2}^{g(Q)}}{s_W c_W} \right)^2. \quad (53)$$

We observe $\sigma(gg \rightarrow H_2) \times B(H_2 \rightarrow Z\gamma)$ can be as large as about 8 fb around $\sin \alpha = 0$ at 68 % CL.

In Figs. 14 and 15, we show the correlations between $\sigma(gg \rightarrow H_2) \times B(H_2 \rightarrow \gamma\gamma)$ and $\sigma(gg \rightarrow H_2) \times B(H_2 \rightarrow Z\gamma)$ taking $|\sin \alpha| < 0.1$ and $|\sin \alpha| \geq 0.1$, respectively. In the limits suggested in Eq. (49) with $N_d = N_s$, we have

$$\frac{\Gamma(H_2 \rightarrow Z\gamma)}{\Gamma(H_2 \rightarrow \gamma\gamma)} \Big|_{\sin \alpha \rightarrow 0} \simeq 2 \left(-t_W + \frac{1}{s_W c_W} \frac{S_{H_2}^{g(Q)}}{S_{H_2}^{\gamma(F)}} \right)^2. \quad (54)$$

When $|\sin \alpha| < 0.1$, we observe

$$\frac{1}{5} \sigma(gg \rightarrow H_2) \times B(H_2 \rightarrow \gamma\gamma) \lesssim \sigma(gg \rightarrow H_2) \times B(H_2 \rightarrow Z\gamma) \lesssim \frac{4}{5} \sigma(gg \rightarrow H_2) \times B(H_2 \rightarrow \gamma\gamma) + 2 \text{ fb}. \quad (55)$$

We find the correlation is strong when $|\sin \alpha| \geq 0.1$ and $|S_{H_2}^{g(Q)}/S_{H_2}^{\gamma(F)}|$ is small, see Figs. 3 and 4. In this case, we find

$$\frac{\sigma(gg \rightarrow H_2) \times B(H_2 \rightarrow Z\gamma)}{\sigma(gg \rightarrow H_2) \times B(H_2 \rightarrow \gamma\gamma)} \simeq 2t_W^2 \simeq 2/3 \quad (56)$$

as shown in Fig. 15 and indicated by Eq. (54).

VI. DISCUSSION

We have performed a “Double Higgcision” – Higgs precision study on both the 125 GeV Higgs boson and a potential diphoton resonance that may appear in the near future data. The recent 750 GeV diphoton resonance serves as a concrete example and we borrow the diphoton resonance data collected in 2015 in our analysis. We have used all the available Higgs boson data from 7 & 8 TeV runs as well as the diphoton cross sections of the 750 GeV boson from the 13 TeV run in 2015.

The important findings and a few comments are summarized as follows:

1. We have divided the analysis into two cases: (i) the width is varied freely and (ii) a broad-width defined by $\Gamma_{H_2} > 40$ GeV is enforced. In the former case, a narrow width is always preferred and the width is of order 1 – 3 GeV. On the other hand, in the broad-width case the width is around 45 GeV. Note that the minimal χ^2 for these two cases only differ by a small amount, which is statistically not significant.
2. As we have shown that $S_{H_1}^{g(Q)}$ and $S_{H_2}^{g(Q)}$ and similarly $S_{H_1}^{\gamma(F)}$ and $S_{H_2}^{\gamma(F)}$ are independent parameters, but, however, they share the same form and with varying VLF mass their ratios $\eta^{g(Q)}$ and $\eta^{\gamma(F)}$ range between 2/3 and 1 for VLF mass from m_{H_2} to infinity. We have shown the results of our analysis for these two representative values of η s in **F4-2** and **F4-3** fits, which have similar features.
3. We have also demonstrated the extreme case of η s equal to zero, i.e., the VLFs do not affect the gluon-fusion production of H_1 and the decays of H_1 into photons and gluons. In such a scenario, the effect of H_2 on H_1 Higgs boson data is only via the mixing angle $\cos \alpha$. Also, in the case the decays of H_2 into other modes such as WW , ZZ , and $t\bar{t}$ are only via the mixing with H_1 . The best-fit shown allows a very tiny mixing angle $|\sin \alpha| \sim 10^{-4}$ such that the decays of $H_2 \rightarrow WW, ZZ, t\bar{t}$ are negligible. If this is the case in the future data, there arises one immediate question why the mixing angle α is so tiny. This should be accommodated in any models for the 750 GeV diphoton excess.
4. In the fits of **F4-2** and **F4-3**, the mixing angles are not too small and of order 10^{-2} . The cross sections of H_2 into $WW, ZZ, t\bar{t}$ are not negligible and demonstrate the cross

sections in the ratio of $4 : 2 : 1$, because of they are all proportional to the square of the SM couplings and $\sin \alpha$.

5. Both narrow and broad-width options in all three **F4** fits, the $\Gamma_{H_2}^{\text{non-SM}}$ dominates the total width Γ_{H_2} of H_2 , especially in the broad-width case the non-SM decay accounts for more than 99% branching ratio.
6. Should the WW , ZZ , $Z\gamma$ or $t\bar{t}$ modes of the H_2 be observed in near future, they would be extremely useful to tell the information on the VLFs.
7. If we assume that VLQs are weak isospin singlets and/or doublets, we can make more explicit and specific predictions on $H_2 \rightarrow WW, ZZ, Z\gamma$, which are shown in Figs. 11-15. Discovery or upper bounds on the branching ratios of 750 GeV boson into these channels would shed more light on the nature of the VLQs in the loop. This could be complementary to the direct search for VLQs at the LHC through QCD interactions, keeping in mind that the decays of VLQs would be more model dependent.
8. Our procedure can be applied in the future discovery of a new resonance in the loop-induced diphoton and/or $Z\gamma$ channels, in particular, taking into account a possible mixing with the SM Higgs boson. Through this work, we demonstrate in detail how to carry out the relevant analysis in a proper way.

ACKNOWLEDGMENTS

This work is supported in part by National Research Foundation of Korea (NRF) Research Grant NRF-2015R1A2A1A05001869, and by the NRF grant funded by the Korea government (MSIP) (No. 2009-0083526) through Korea Neutrino Research Center at Seoul National University (PK). The work of K.C. was supported by the MoST of Taiwan under Grants No. NSC 102-2112-M-007-015-MY3.

Appendix A: Decay widths of H_2 into $Z\gamma$, ZZ , and WW

In this appendix, we present the explicit forms for the decay widths of H_2 into $Z\gamma$, ZZ , and WW including the mixing between the SM Higgs boson and the singlet scalar.

The amplitude for the decay process $H_2 \rightarrow Z(k_1, \epsilon_1) \gamma(k_2, \epsilon_2)$ can be written as

$$\mathcal{M}_{Z\gamma H_2} = -\frac{\alpha}{2\pi v} S_{H_2}^{Z\gamma} [k_1 \cdot k_2 \epsilon_1^* \cdot \epsilon_2^* - k_1 \cdot \epsilon_2^* k_2 \cdot \epsilon_1^*] \quad (\text{A.1})$$

where $k_{1,2}$ are the 4-momenta of the Z boson and the photon, respectively, and $\epsilon_{1,2}$ are their polarization vectors. We note that $2k_1 \cdot k_2 = M_{H_2}^2 - M_Z^2$. The form factor $S_{H_2}^{Z\gamma}$ is given by the sum

$$S_{H_2}^{Z\gamma} = \sin \alpha S_{H_2}^{Z\gamma(\text{SM})} + \cos \alpha S_{H_2}^{Z\gamma(F)}$$

with $S_{H_2}^{Z\gamma(\text{SM})} \simeq -0.0771 - 1.805i$. The VLF contribution $S_{H_2}^{Z\gamma(F)}$ is model dependant and it is given by Eq. (44) in the context of $SU(2)_L$ -doublet and singlet VLFs discussed in Section V. Then, the decay width of H_2 into $Z\gamma$ is given by

$$\Gamma(H_2 \rightarrow Z\gamma) = \frac{M_{H_2}^3 \alpha^2}{128\pi^3 v^2} \left(1 - \frac{M_Z^2}{M_{H_2}^2}\right)^3 |S_{H_2}^{Z\gamma}|^2, \quad (\text{A.2})$$

with

$$|S_{H_2}^{Z\gamma}|^2 = \sin^2 \alpha |S_{H_2}^{Z\gamma(\text{SM})}|^2 + 2 \cos \alpha \sin \alpha S_{H_2}^{Z\gamma(F)} \Re(S_{H_2}^{Z\gamma(\text{SM})}) + \cos^2 \alpha (S_{H_2}^{Z\gamma(F)})^2 \quad (\text{A.3})$$

assuming that the VLF mass satisfies $m_F > M_{H_2}/2$ so that $S_{H_2}^{Z\gamma(F)}$ becomes real.

The amplitude for the decay process $H_2 \rightarrow V(k_1, \epsilon_1) V(k_2, \epsilon_2)$ can be written as

$$\mathcal{M}_{VVH_2} = \sin \alpha \mathcal{M}_{VVH_2}^{(0)} + \cos \alpha \mathcal{M}_{VVH_2}^{(1)}.$$

In the leading order neglecting the SM one-loop contributions to the hWW vertex, the tree-level and one-loop amplitudes are given by Eq. (46):

$$\begin{aligned} \mathcal{M}_{WWH_2}^{(0)} &= -g M_W \epsilon_1^* \cdot \epsilon_2^*, \quad \mathcal{M}_{ZZH_2}^{(0)} = -\frac{g M_W}{c_W^2} \epsilon_1^* \cdot \epsilon_2^*; \\ \mathcal{M}_{VVH_2}^{(1)} &= -\frac{\alpha}{2\pi v} S_{H_2}^{VV(F)} [k_1 \cdot k_2 \epsilon_1^* \cdot \epsilon_2^* - k_1 \cdot \epsilon_2^* k_2 \cdot \epsilon_1^*]. \end{aligned}$$

The VLF contributions $S_{H_2}^{ZZ(F)}$ and $S_{H_2}^{WW(F)}$ are model dependent and they are given by Eqs. (47) and (48), respectively, in the context discussed in Section V. Finally, the decay width of H_2 into VV is given by

$$\Gamma(H_2 \rightarrow VV) = \frac{\delta_V}{32\pi M_{H_2}} \sum |\mathcal{M}_{VVH_2}|^2 \sqrt{1 - \frac{4M_V^2}{M_{H_2}^2}} \quad (\text{A.4})$$

with $\delta_W = 2$ and $\delta_Z = 1$. For the amplitude squared, explicitly, we obtain

$$\begin{aligned} \sum |\mathcal{M}_{WWH_2}|^2 &= \sin^2 \alpha g^2 M_W^2 \left[3 - \frac{M_{H_2}^2}{M_W^2} + \frac{M_{H_2}^4}{4M_W^4} \right] \\ &\quad + \sin \alpha \cos \alpha \frac{gM_W \alpha}{\pi v} \left[-3M_W^2 + \frac{3M_{H_2}^2}{2} \right] S_{H_2}^{WW(F)} \\ &\quad + \cos^2 \alpha \frac{\alpha^2}{4\pi^2 v^2} \left[3M_W^4 - 2M_W^2 M_{H_2}^2 + \frac{M_{H_2}^4}{2} \right] \left(S_{H_2}^{WW(F)} \right)^2 ; \end{aligned} \quad (\text{A.5})$$

$$\begin{aligned} \sum |\mathcal{M}_{ZZH_2}|^2 &= \sin^2 \alpha \frac{g^2 M_W^2}{c_W^4} \left[3 - \frac{M_{H_2}^2}{M_Z^2} + \frac{M_{H_2}^4}{4M_Z^4} \right] \\ &\quad + \sin \alpha \cos \alpha \frac{gM_W \alpha}{c_W^2 \pi v} \left[-3M_Z^2 + \frac{3M_{H_2}^2}{2} \right] S_{H_2}^{ZZ(F)} \\ &\quad + \cos^2 \alpha \frac{\alpha^2}{4\pi^2 v^2} \left[3M_Z^4 - 2M_Z^2 M_{H_2}^2 + \frac{M_{H_2}^4}{2} \right] \left(S_{H_2}^{ZZ(F)} \right)^2 . \end{aligned} \quad (\text{A.6})$$

-
- [1] G. Aad *et al.* [ATLAS Collaboration], “Observation of a new particle in the search for the Standard Model Higgs boson with the ATLAS detector at the LHC,” Phys. Lett. B **716**, 1 (2012) [arXiv:1207.7214 [hep-ex]].
 - [2] S. Chatrchyan *et al.* [CMS Collaboration], “Observation of a new boson at a mass of 125 GeV with the CMS experiment at the LHC,” Phys. Lett. B **716**, 30 (2012) [arXiv:1207.7235 [hep-ex]].
 - [3] J. Chang, K. Cheung and C. T. Lu, Phys. Rev. D **93**, no. 7, 075013 (2016) doi:10.1103/PhysRevD.93.075013 [arXiv:1512.06671 [hep-ph]].
 - [4] B. Lenzi (ATLAS collaboration), “Search for a high mass diphoton resonance using the ATLAS detector,” a talk at the 38th International Conference on High Energy Physics (ICHPE2016); C. Rovelli (CMS collaboration), “Search for BSM physics in di-photon final states at CMS,” a talk at the 38th International Conference on High Energy Physics (ICHPE2016).
 - [5] S. Choi, S. Jung and P. Ko, “Implications of LHC data on 125 GeV Higgs-like boson for the Standard Model and its various extensions,” JHEP **1310** (2013) 225 [arXiv:1307.3948].
 - [6] K. Cheung, P. Ko, J. S. Lee and P. Y. Tseng, JHEP **1510**, 057 (2015) doi:10.1007/JHEP10(2015)057 [arXiv:1507.06158 [hep-ph]].
 - [7] K. Cheung, P. Ko, J. S. Lee, J. Park and P. Y. Tseng, arXiv:1512.07853 [hep-ph].

- [8] J. S. Lee, A. Pilaftsis, M. S. Carena, S. Y. Choi, M. Drees, J. R. Ellis and C. E. M. Wagner, “CPsuperH: A Computational tool for Higgs phenomenology in the minimal supersymmetric standard model with explicit CP violation,” *Comput. Phys. Commun.* **156** (2004) 283 [hep-ph/0307377].
- [9] S. Dittmaier *et al.* [LHC Higgs Cross Section Working Group Collaboration], doi:10.5170/CERN-2011-002 arXiv:1101.0593 [hep-ph].
- [10] K. Cheung, J. S. Lee and P. Y. Tseng, “Higgs Precision (Higgcision) Era begins,” *JHEP* **1305** (2013) 134 [arXiv:1302.3794 [hep-ph]].
- [11] K. Cheung, J. S. Lee and P. Y. Tseng, “Higgcision Updates 2014,” arXiv:1407.8236 [hep-ph].
- [12] ATLAS Collaboration, “Search for resonances decaying to photon pairs in 3.2 fb1 of pp collisions at $\sqrt{s} = 13$ TeV with the ATLAS detector”, ATLAS-CONF-2015-081 (Dec. 2015).
- [13] CMS Collaboration, “Search for new physics in high mass diphoton events in proton-proton collisions at 13 TeV”, CMS PAS EXO-15-004 (Dec. 2015).
- [14] ATLAS Collaboration, “Search for diboson resonances in the $llqq$ final state in pp collisions at $\sqrt{s} = 13$ TeV with the ATLAS detector, ATLAS-CONF-2015-071 (Dec. 2015); ATLAS Collaboration, “Search for WW/WZ resonance production in the $\ell\nu qq$ final state at $\sqrt{s} = 13$ TeV with the ATLAS detector at the LHC, ATLAS-CONF-2015-075 (Dec. 2015).
- [15] ATLAS Collaboration, “A search for $t\bar{t}$ resonances using lepton-plus-jets events in proton-proton collisions at $\sqrt{s} = 8$ TeV with the ATLAS detector”, arXiv: 1505.07018 (May 2015).
- [16] ATLAS Collaboration, “Search for new phenomena in the dijet mass distribution using pp collision data at $\sqrt{s} = 8$ TeV with the ATLAS detector”, arXiv:1407.1376
- [17] G. Aad *et al.* [ATLAS Collaboration], “Searches for Higgs boson pair production in the $hh \rightarrow b\bar{b}\tau\tau, \gamma\gamma WW^*, \gamma\gamma b\bar{b}, b\bar{b}b\bar{b}$ channels with the ATLAS detector,” *Phys. Rev. D* **92** (2015) 092004 doi:10.1103/PhysRevD.92.092004 [arXiv:1509.04670 [hep-ex]].
- [18] LHC Higgs Cross Section Working Group: Higgs cross sections and decay branching ratios “<https://twiki.cern.ch/twiki/bin/view/LHCPhysics/WebHome>”.

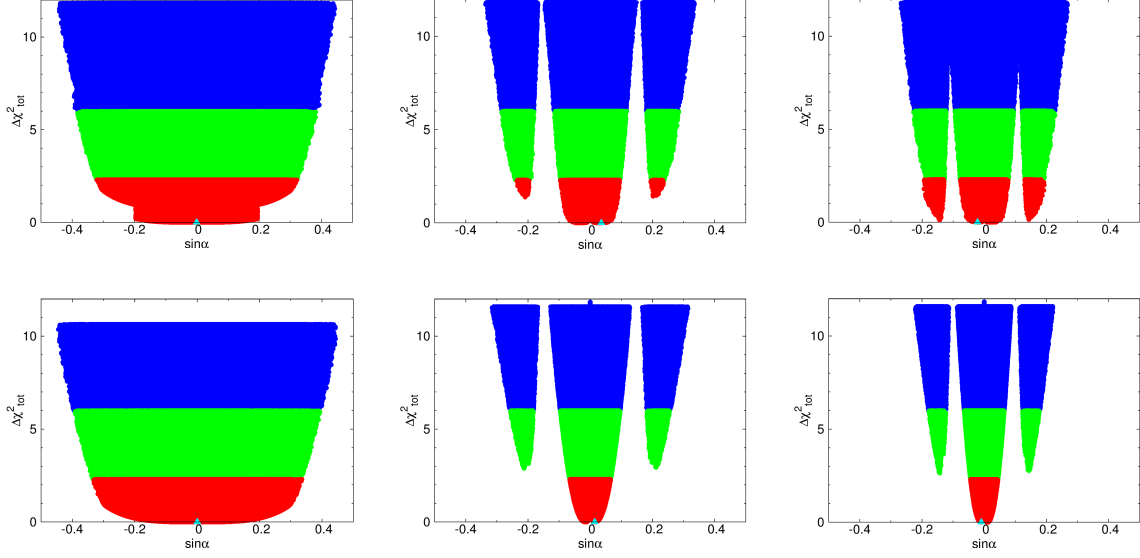


FIG. 1. **F4 fits:** Plots of $\Delta\chi^2$ vs $\sin\alpha$ for the **F4-1** (left), **F4-2** (middle), and **F4-3** (right) fits. In the upper row, we consider the full range of Γ_{H_2} while, in the lower row, we consider the wide-width case requiring $\Gamma_{H_2} \geq 40$ GeV. The regions shown are for $\Delta\chi^2 = 2.3$ (red), 5.99 (green), and 11.83 (blue) above the minimum. The triangles denote the corresponding minima.

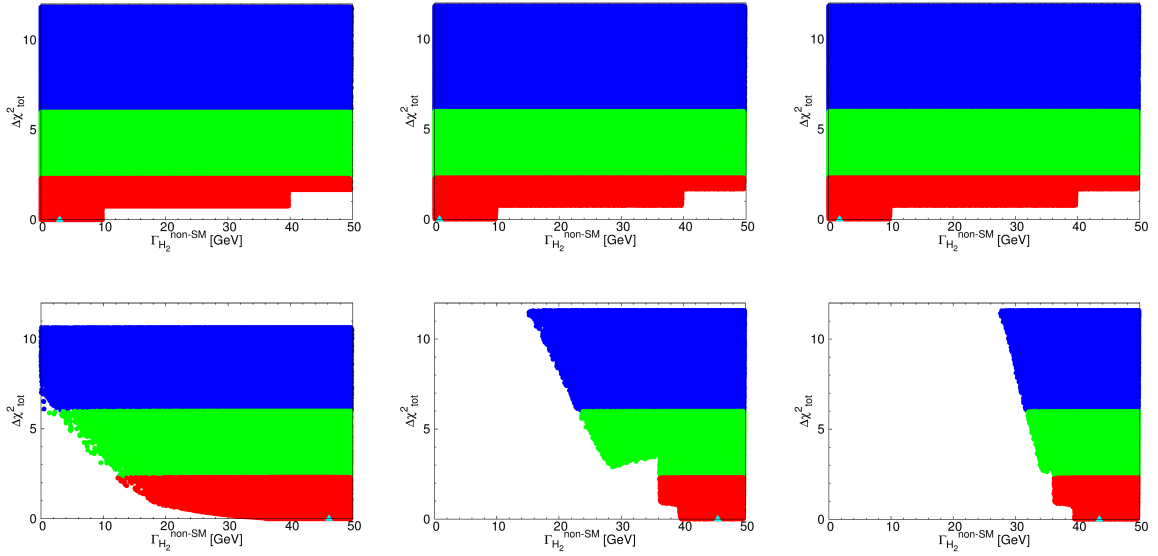


FIG. 2. **F4 fits:** The same as in FIG. 1 but for $\Delta\chi^2$ vs $\Gamma_{H_2}^{\text{non-SM}}$.

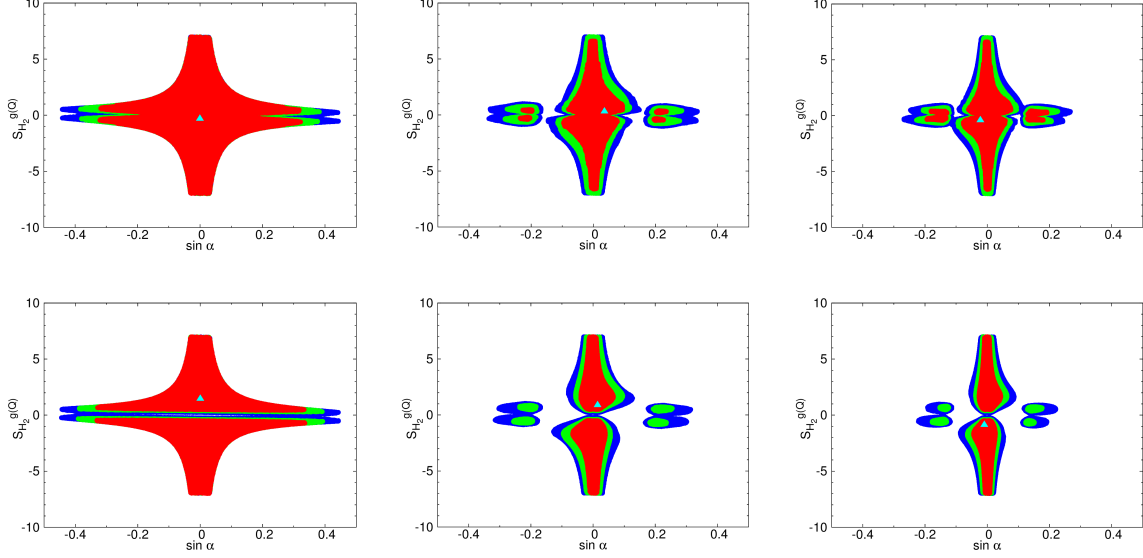


FIG. 3. **F4 fits:** The CL regions for the **F4-1** (left), **F4-2** (middle), and **F4-3** (right) fits in the $(\sin \alpha, S_{H_2}^{g(Q)})$ plane. In the upper row, we consider the full range of Γ_{H_2} while, in the lower row, we consider the wide width case requiring $\Gamma_{H_2} \geq 40$ GeV. In all the frames, we impose the diboson, $t\bar{t}$, and dijet constraints: $\sigma(pp \rightarrow H_2) \times B(H_2 \rightarrow VV) \lesssim 150$ fb at 13 TeV, $\sigma(pp \rightarrow H_2) \times B(H_2 \rightarrow t\bar{t}) \lesssim 0.5$ pb at 8 TeV, and $\sigma(pp \rightarrow H_2) \times B(H_2 \rightarrow gg) \lesssim 1$ pb at 8 TeV. The contour regions shown are for $\Delta\chi^2 = 2.3$ (red), 5.99 (green), and 11.83 (blue) above the minimum, which correspond to confidence levels of 68.3%, 95%, and 99.7%, respectively. The triangles in the upper row denote the minima over the full range of Γ_{H_2} , while those in the lower row the minima obtained under the assumption of $\Gamma_{H_2} \geq 40$ GeV.

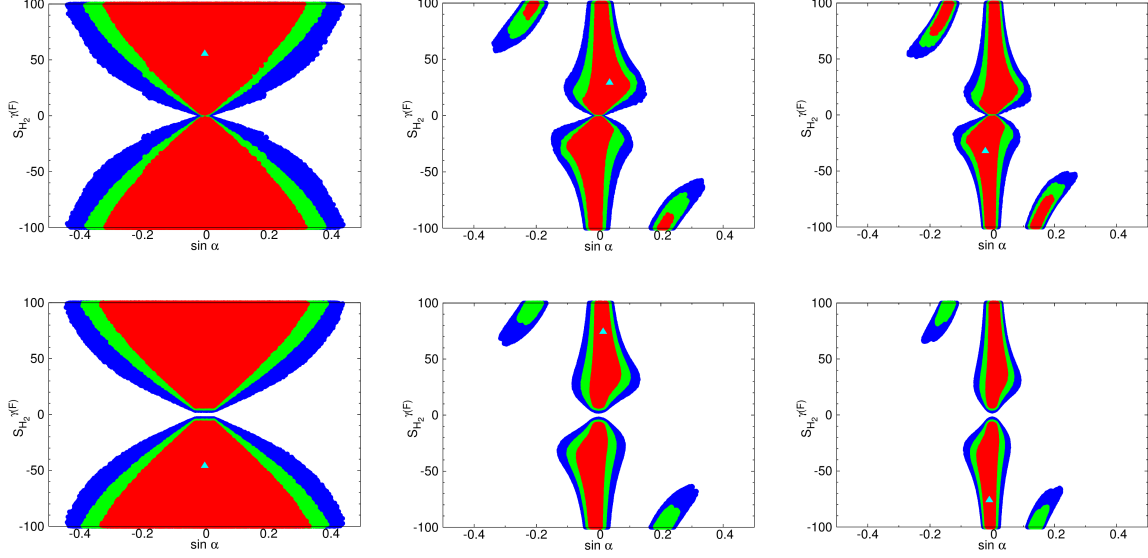


FIG. 4. **F4 fits:** The same as in FIG. 3 but for the CL regions in the $(\sin \alpha, S_{H_2}^{\gamma(F)})$ plane.

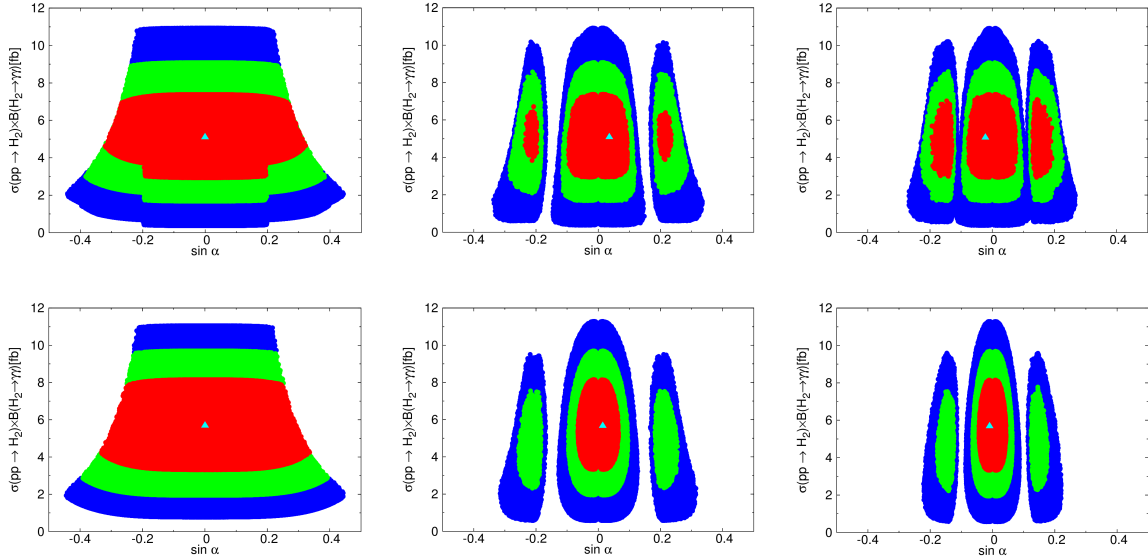


FIG. 5. **F4 fits:** The same as in FIG. 3 but for the CL regions in the $(\sin \alpha, \sigma(gg \rightarrow H_2) \times B(H_2 \rightarrow \gamma\gamma))$ plane.

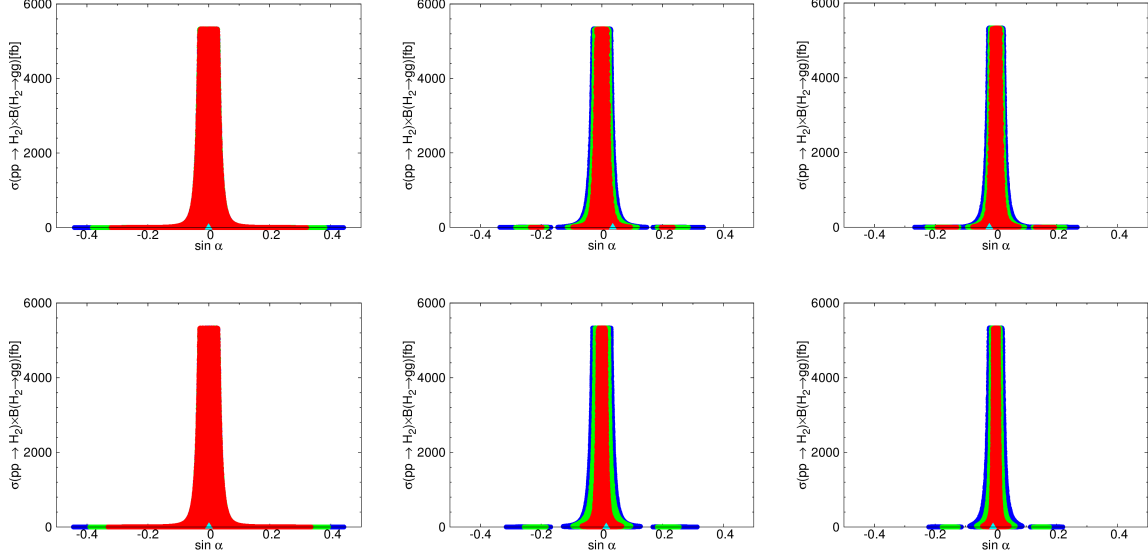


FIG. 6. **F4 fits:** The same as in FIG. 3 but for the CL regions in the $(\sin \alpha, \sigma(gg \rightarrow H_2) \times B(H_2 \rightarrow gg))$ plane.

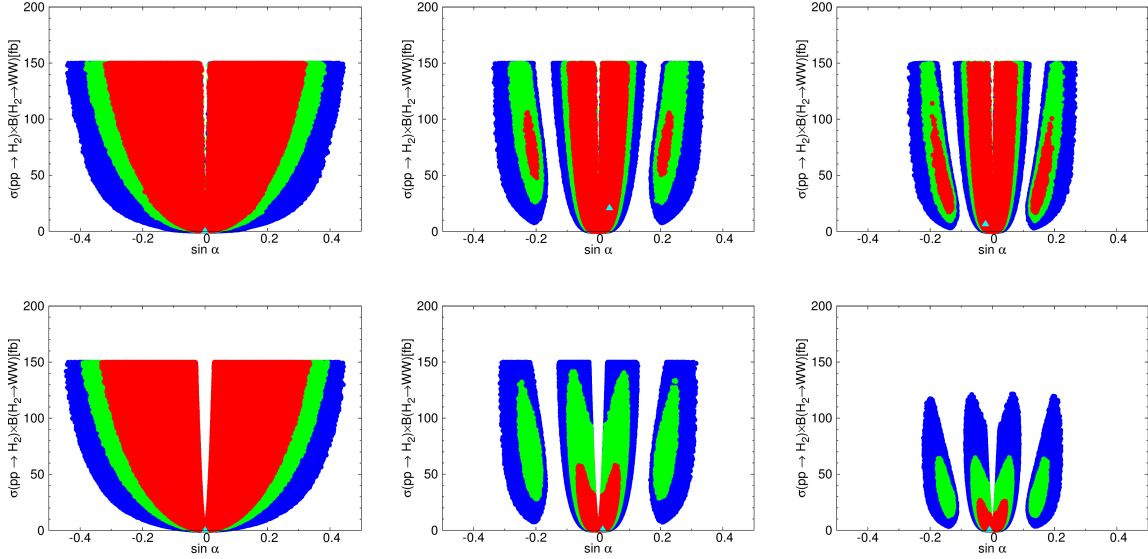


FIG. 7. **F4 fits:** The same as in FIG. 3 but for the CL regions in the $(\sin \alpha, \sigma(gg \rightarrow H_2) \times B(H_2 \rightarrow WW))$ plane.

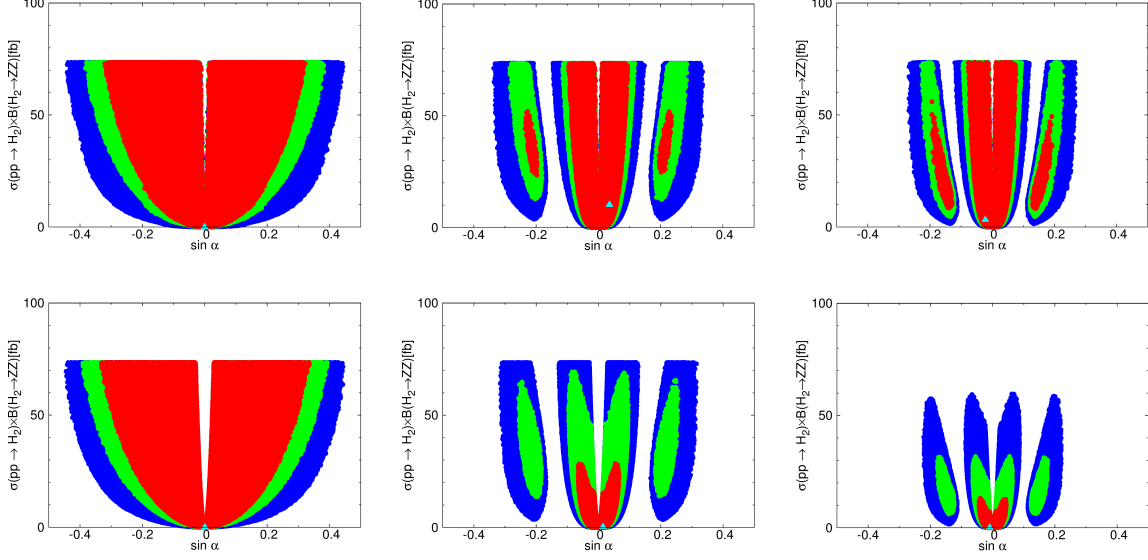


FIG. 8. **F4 fits**: The same as in FIG. 3 but for the CL regions in the $(\sin \alpha, \sigma(gg \rightarrow H_2) \times B(H_2 \rightarrow ZZ))$ plane.

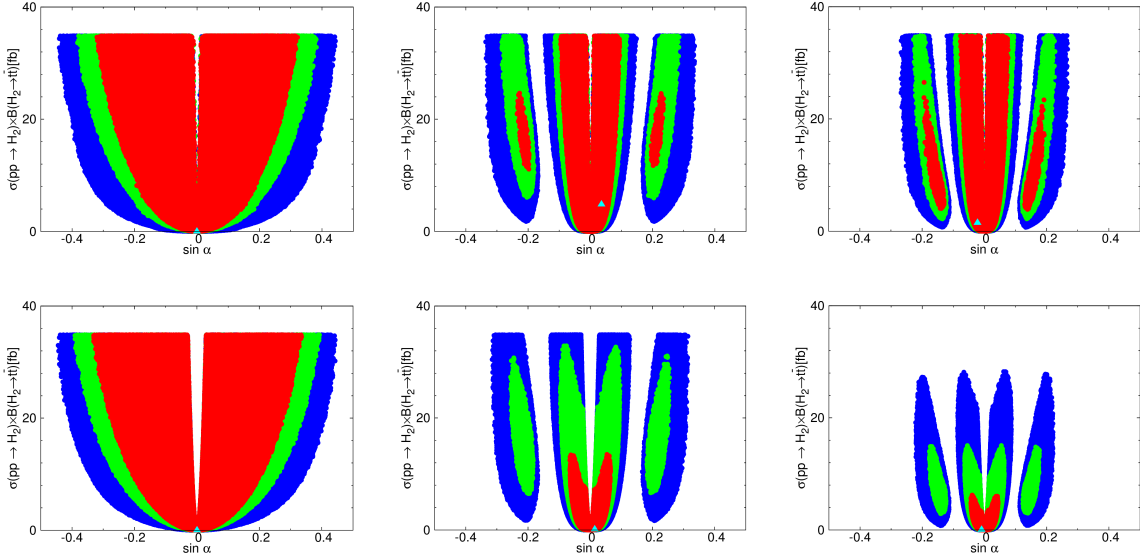


FIG. 9. **F4 fits**: The same as in FIG. 3 but for the CL regions in the $(\sin \alpha, \sigma(gg \rightarrow H_2) \times B(H_2 \rightarrow t\bar{t}))$ plane.

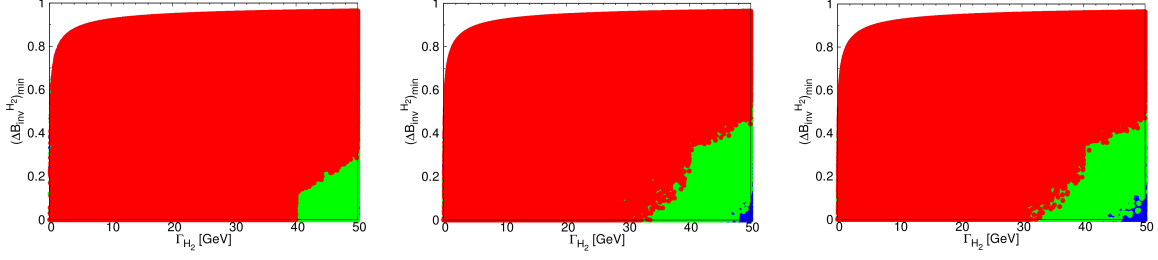


FIG. 10. **F4 fits:** The CL regions for the **F4-1** (left), **F4-2** (middle), and **F4-3** (right) fits in the $(\Gamma_{H_2}, (\Delta B_{\text{inv}}^{H_2})_{\text{min}})$ plane. The colors are the same as in FIG. 3. See text for the definition of $(\Delta B_{\text{inv}}^{H_2})_{\text{min}}$.

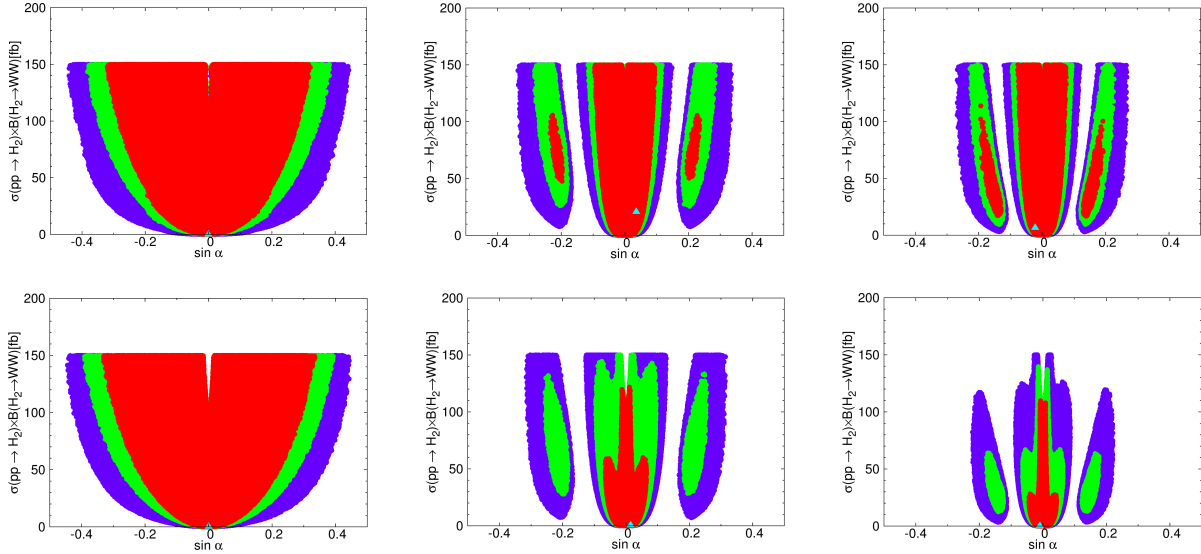


FIG. 11. **VLQ-W/Z:** The same as in FIG. 7 but including the VLQ-loop induced contributions to $B(H_2 \rightarrow WW)$ in the presence of interactions between VLQs and W/Z bosons discussed in Section V. We are taking the limits in Eq. (49) and $N_d = N_s$.

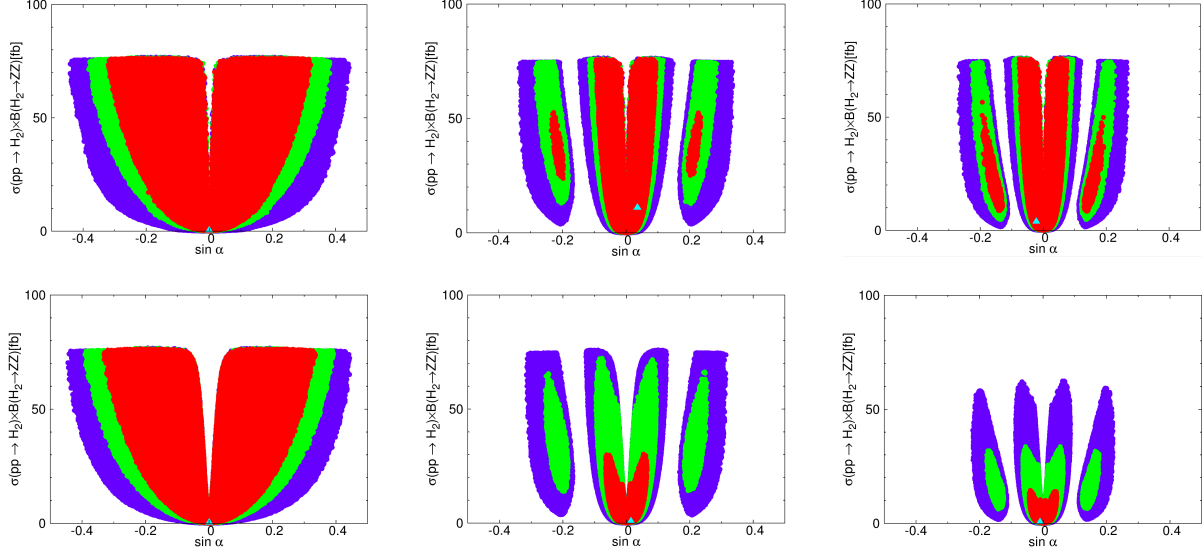


FIG. 12. **VLQ-W/Z**: The same as in FIG. 8 but including the VLQ-loop induced contributions to $B(H_2 \rightarrow ZZ)$ in the presence of interactions between VLQs and W/Z bosons discussed in Section V. We are taking the limits in Eq. (49) and $N_d = N_s$.

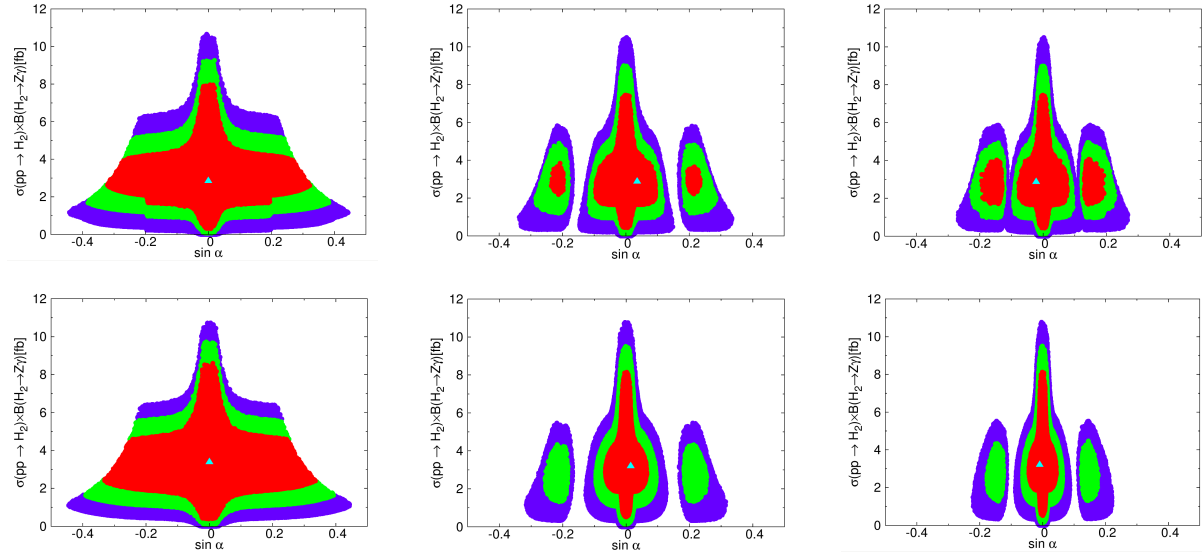


FIG. 13. **VLQ-W/Z**: The same as in FIG. 3 but for the CL regions in the $(\sin \alpha, \sigma(gg \rightarrow H_2) \times B(H_2 \rightarrow Z\gamma))$ plane, including the VLQ-loop induced contributions in the presence of interactions between VLQs and W/Z bosons discussed in Section V. We are taking the limits in Eq. (49) and $N_d = N_s$.

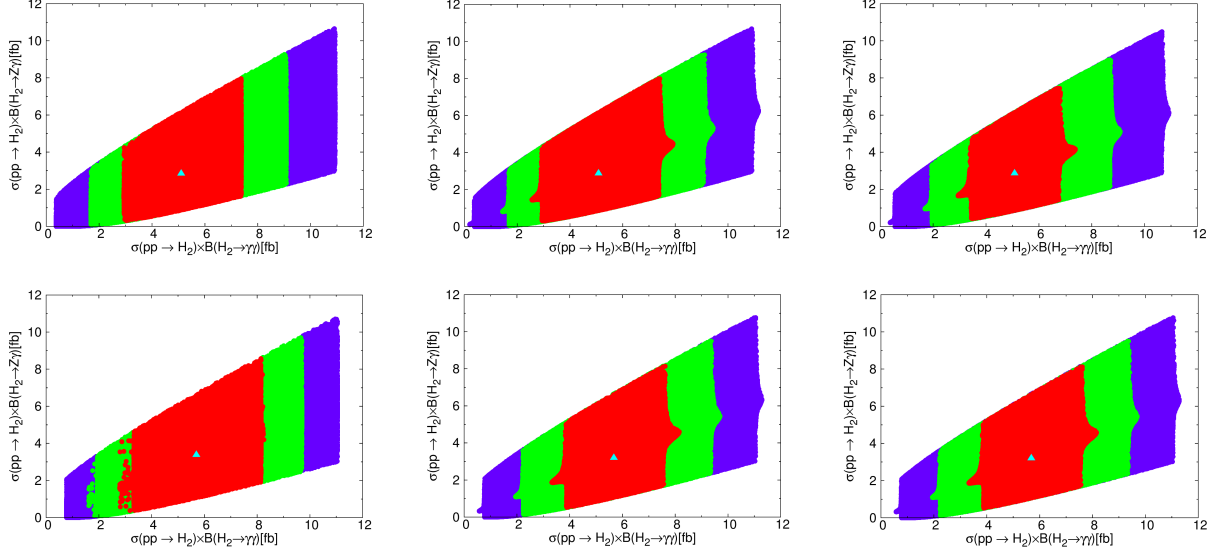


FIG. 14. **VLQ-W/Z**: The CL regions for the correlations between $\sigma(gg \rightarrow H_2) \times B(H_2 \rightarrow \gamma\gamma)$ and $\sigma(gg \rightarrow H_2) \times B(H_2 \rightarrow Z\gamma)$ when $|\sin \alpha| < 0.1$, including the VLQ-loop induced contributions in the presence of interactions between VLQs and W/Z bosons discussed in Section V. We are taking the limits in Eq. (49) and $N_d = N_s$. The colors are the same as in FIG. 3.

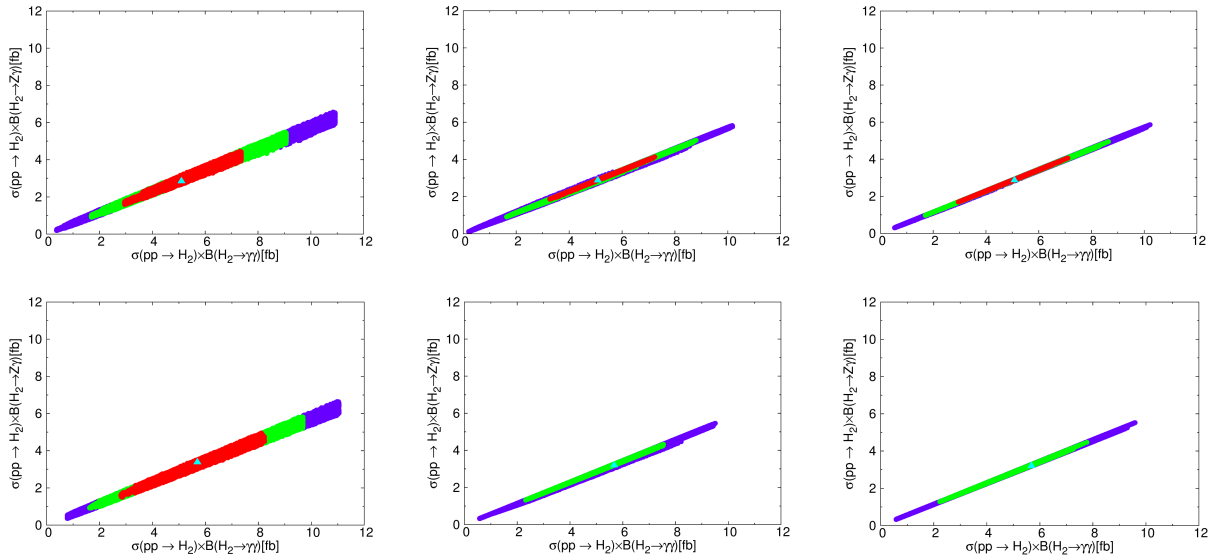


FIG. 15. **VLQ-W/Z**: The same as in FIG. 14 but for $|\sin \alpha| \geq 0.1$.